Metal-Free Carbon-Based Nanomaterials as Sustainable Catalysts: Insights from Synthesis to Applications in Electrochemical Sensing, Biomass Valorization and Fine Chemical Synthesis

Vishal Bharati Jaryal[a], Alberto Villa[b], Neeraj Gupta[a]*

[a]Department of Chemistry and Chemical Science, School of Physical and Material Sciences, Central University of Himachal Pradesh, Dharamshala (Himachal Pradesh) – 176202, India.

[b]Dipartimento di Chimica Universita` degli Studi di Milano Via golgi 19, 20133 Milano, Italy

CONSPECTUS

The development of cutting-edge catalysts is critical in material science and engineering for sustainable development. Metals have always been widely used to generate conducting materials for developing various chemical and biosensors. They can also be deposited as nanoparticles on different supports for making catalysts in chemical and biomass conversions. However, sustainable processes more often use noble-metal-based materials, but their use is limited due to the high cost, limited availability, low selectivity and poor durability. Carbon-based nanomaterials have become the focus of researchers over the last thirty years and are used either as a catalyst support or metal-free catalyst in various chemical conversions. Carbons are highly anticipated as state-of-the-art materials due to their high specific surface area, well-developed pore distribution, high conductivity along with tuneable functional groups. Significant advancements have been made in the field of “metal-free catalysis” by using carbon-based materials.

This account summarises various strategies proposed by our group to design metal-free carbon-based catalysts for electrochemical sensing, biomass valorization and synthesis of value-added specialty chemicals. Also, “metal-free” point-of-care devices are fabricated to provide affordable healthcare services to the user end. The materials are designed with the help of graphitic carbon nitride, reduced graphene oxide, Janus 2D carbon nanomaterials, ultra-dispersed diamonds and carbon nanotubes. The key strategies employed for designing these catalysts are electrospinning, thermal annealing, covalent tagging, surface modification, heteroatom doping and heterogenization. Furthermore, their efficacy can be improved by building composites with other non-toxic metal-free materials and incorporating defects with the help of non-metals. Finally, we share some of our

knowledge and insights on current challenges and future research directions in this emerging field.

1. Introduction

Industrialization in recent years has brought economic prosperity but additionally, it has begun to have a negative impact on the environment, posing serious difficulties[1]. Although, chemistry has substantially improved people's quality of life by producing thousands of commercially important products. However, the ecosystem is being deteriorated as a result of the excessive utilization of natural resources and the production of undesired toxic chemicals[2]. Therefore, one of the key research goals in the field of chemistry is to develop efficient, sustainable and selective approaches. Sustainability aims to meet the demands of the present generation without compromising the needs of future generation[2] and the use of sustainable catalysts should be encouraged for future developments in this regard.

Catalysis has impacted the chemical industry and the academic research and significantly influenced our lives[3]. Heterogeneous catalysis governs various chemical and energy transformation processes[4]. A significant proportion (around 80%) of various processes in chemical industries relies on catalytic reactions[5]. Both homogeneous and heterogeneous catalytic processes have been dominated by the use of metal or metal oxide-based catalysts, especially noble metals such as Pt, Pd and Ru[5,6]. However, the usage of metals raises concerns about the overall viability of the method, pointing to the adoption of alternative metal-free analogues[7–9]. Though, there have been significant efforts to better utilize metals in heterogenous catalysts by increasing activity per site. This can be achieved by reducing the particle size even to the extent of being single atom-site catalysts, and by improving their stability and reactivation procedures[5,10]. Few metal ions from the catalyst may even leak into the environment through catalytic processes causing various types of pollution. In order to stop this, a new class of materials is getting the focus of researchers and environmentalists where metal is completely missing. Development of metal free materials is not new and it is preceded by a class of metal free homogeneous catalysts known as "organo-catalysts". The use of cinchona alkaloids for the HCN (hydrogen cyanide) addition to aldehydes, published in 1912 by Breding and Fiske[11], is one of the earliest known organocatalyzed reactions. The popularity of these metal free catalysts/materials has grown in recent years owing to the economic, safety and environmental concerns[12]. Carbon-based materials have proven to be one of the most successful materials in this regard[13,14].

There are some conceptual grounds that characterize carbon as a viable catalyst. It is a semi-metal with a small proportion of metallic electrons that can be found either at the surface in delocalized (graphitic) or localized (bent nano carbons) forms in its sp^2 hybridized state[15]. Carbon nanostructures without metal components have been intensively examined and studied in catalysis as part of an effort toward green and sustainable chemistry[16]. Carbon nanomaterials are also known as metal-free catalysts and attracted more attention due to their excellent performance in a variety of chemical reactions such as reduction of nitrobenzene and oxygen reduction reaction[17] in fuel cells, oxidation of alcohols, alkynes, thiols and sulphides[18].

2. Scope of the Account

Biomass valorization has given a new dimension to the entire product generation processes. The plant-derived waste biomass can be successfully utilized for the production of value-added materials and fine chemicals. This account summarises the fabrication of metal-free carbon-based catalysts for fine chemical synthesis and biomass valorisation as a substitute to metal-based analogues. It aims to provide a detailed insight on the identification of catalytically active sites involved in the synthesis of a variety of organic molecules. The designing of such active sites for performing key biomass conversion reactions such as oxidation of glycerol, selective dehydration of fructose and transesterification of triglycerides have been discussed in detail. A comprehensive analysis of such reactions with the mechanistic pathway involved will enhance the existing knowledge regarding these reactions. Besides, methods for improving the sensitivity of carbon materials towards a particular bio-analyte are explained. Advancements have been made for enhancing the conductivity and electrocatalytic properties of these carbon materials by incorporation of heteroatoms in their matrix.

The research gaps of metal-free carbon-based catalysts are identified and various sophisticated approaches have been proposed for utilizing these carbo-catalysts for the development of POC devices for electrochemical sensing of various body fluids. Finally, this account paves the way for expanding the knowledge base to support the use of nanocarbons in sustainable catalysis and environmental chemistry by the application of carbo-catalysis in fine chemical synthesis and biomass valorisation.

3. Incorporation of Key Active Sites in Metal-Free Carbon Materials

Development of effective carbo-catalyst depends upon the incorporation of metal-free key active sites in carbon matrix. Accurate knowledge of the active sites can assist researchers come up with the best preparation conditions of such metal-free materials. Several techniques for determining the nature of the active sites in carbon materials (crystalline and non-crystalline) have been documented in the literature[19,20]. However, all of them have few limitations and there is always a degree of uncertainty associated with the catalytic centres[5,21,22]. Different techniques such as electrospinning, thermal annealing, covalent tagging, surface modification, heteroatom doping, heterogenization, composites and defects (Figure 1) can be adapted to synthesize these metal-free carbon catalysts and the main strategies recently used by our group are described in the succeeding sections.

3.1 Electrospinning

Electrospinning is a quick and easy way to make continuous polymeric nanofibers having high surface roughness due to a large surface-to-volume ratio[23,24]. It can produce masses of nanofibrous yarns, protective gears and random mats due to its simplicity and compatibility to a wide range of polymers.

A high-voltage potential is applied to the solution of a polymer kept at the tip of an electrode. The electrostatic repulsion over the surface of polymer solution triggers the generation of a jet at the end of the solution droplet in the form of a Taylor cone [31–33]. An electric bias is applied to the grounded collection plate from the tip of a polymer solution filled syringe resulting in the formation of electrospun nanofibers. The texture of these electrospun nano fibres can be fine-tuned by controlling the molecular weight of the polymer solution, viscosity as well as the applied voltage[34,35]. These organic polymers with carbon, hydrogen and other atoms (N, O or S) can be converted into carbonaceous materials after the removal of undesirable atoms. One typical method used to remove other atoms from this organic matter is thermal annealing at high temperatures[36]. This process breaks the covalent linkages present in the organic molecules leading to the loss of elements other than carbon. The carbon rich residue reorganises itself into a new form of carbon material.

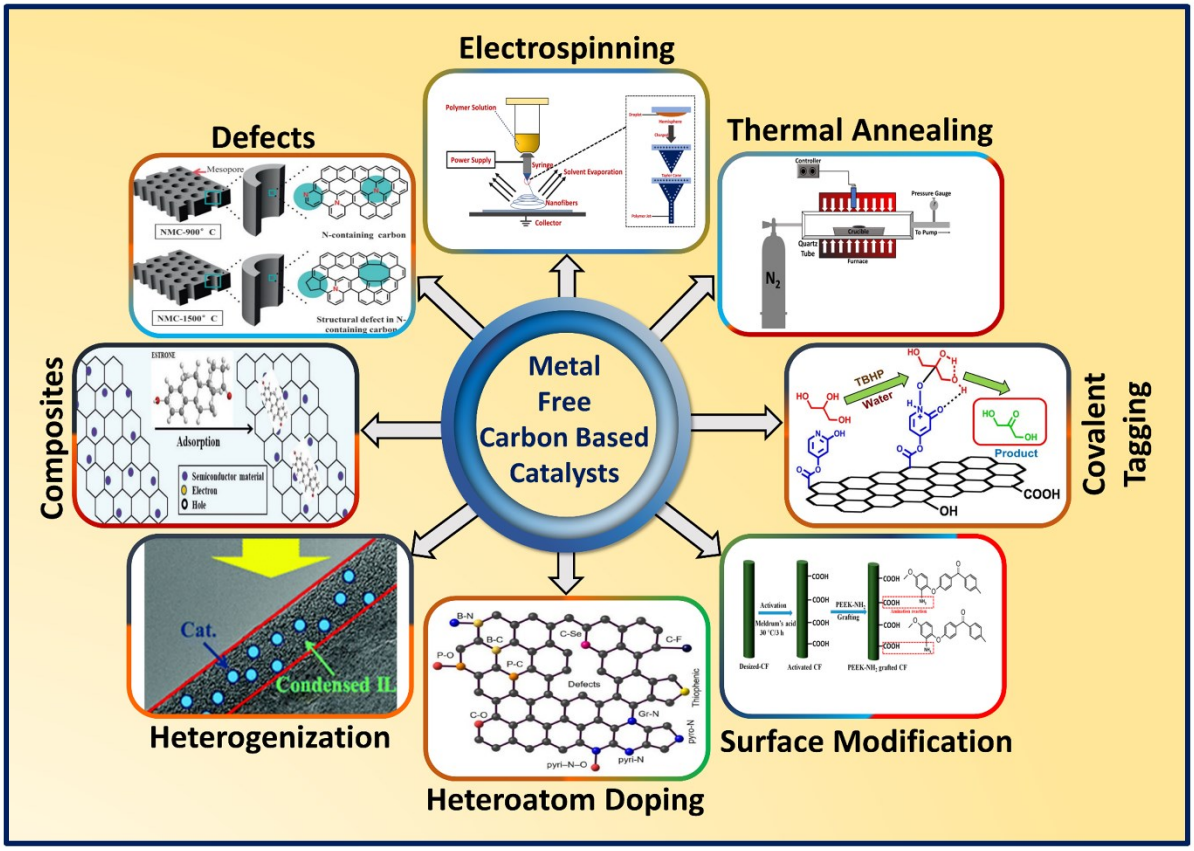

Figure 1. Different methodologies for preparing metal – free carbon catalysts for various applications. Portions of this figure have been reprinted with permission from ref[25–30].

3.2 Thermal Annealing

There is an enormous variety of possible carbon - containing structures and morphologies with broad applications due to the fact that carbon have a variety of hybridisation states including sp, sp^2 and sp^3. Moreover, the degree of graphitization of these carbon-materials can be enhanced, in general, by a traditional method which involves thermal annealing at high temperatures (>2000 ^oC)[37]. The Marsh-Griffiths model[38] has provided a detailed description of the potential changes that might take place in carbon structures during the annealing process. Numerous carbon materials[39,40], such as carbon fibres, carbon soot and carbon nanotubes, have their high temperature annealing processes thoroughly studied. High temperature annealing has a dramatic effect on the morphology of carbon materials, converting them into structures with well-defined shapes.

3.3 Surface Modification

The properties of carbon materials can be significantly tuned by controlling their surface functional groups. Carbon, nitrogen and sulfur[41] containing organic functional groups can be covalently attached to the surface of carbon catalysts. The chemical inertness of carbon materials makes the covalent attachment of functional groups a challenging task. Oxidation and reduction are commonly used techniques for creating surface functional groups for the attachment of various organic molecules. Oxidation can be performed with oxygen gas, peracids as well as strong acids (HNO_3 and $H_2SO_{4)}$. Similarly, reduction can be performed with the help of various reducing agents such as H_2, CO and SO_2. The use of strong oxidants can compromise the integrity of chemical and porous structures of carbon materials. Therefore, other techniques such as diazotization can be used to functionalize them to preserve these properties[42]. This method provides a high level of functional group coverage on carbon surfaces. The insertion of polar groups such as -OH and -COOH through oxides increases the hydrophilicity of carbon material that are generally hydrophobic in nature[43,44]. Therefore, the stability of these materials in aqueous media is improved by treating them with concentrated acids or strong oxidants. It leads to the formation of oxygen-containing functionalities such as hydroxyl or carboxyl groups on their surface[45,46]. These oxygen containing functionalities results in improved catalytic activity in several cases[47].

3.4 Covalent Tagging

Another way to modify the carbon surface and insert key active sites in carbon materials is the covalent tagging with organic molecules. The groups such as hydroxyl, carboxyl, carbonyl, pyridinic, amino and -SH can be functionalised by performing simple organic reactions. For instance, -COOH group can be converted into ester or amide groups by reacting it with other organic molecules. Chemical modification of carboxylic groups is another way to achieve indirect covalent functionalization of carbon surface. Single walled carbon nanotubes have been made more soluble using covalent sidewall functionalization, allowing for the processing and manipulation of otherwise insoluble nanotubes[48]. Possibly, a functionalized nanotube has distinctive mechanical, optical or electrical characteristics from the original nanotube. Direct covalent functionalization in most of the carbon nanomaterials is linked to a shift from sp^2 to sp^3 hybridization and a concurrent loss of conjugation[49,50]. Covalent functionalization has a limitation that the perfect structure of respective carbon materials

such as graphene or CNT is destroyed during the process leading to significant changes in their physical properties.

3.5 Heteroatom Doping

This is one of the most prominent strategies utilized to improve carbon materials for various applications [51]. Heteroatom doping entails the replacement of a few carbon atoms in a carbon skeleton by various heteroatoms such as boron (B), nitrogen (N), sulfur (S), phosphorus (P) and selenium (Se)[52,53]. The introduction of heteroatoms into the carbon host[54] can modify electrical and other properties due to difference in size and electronegativity[55,56]. This causes charge transfer within the heteroatoms resulting in redistribution of charge among carbon atoms. The heteroatoms can be individually or collectively incorporated into a carbon framework either through the carbonization of precursors rich in heteroatoms or chemical post-modification of parental carbons[57]. Different heteroatom types or even the same heteroatom type in a different bond orientation can give different characteristics to carbon[58].

3.6 Heterogenization

Homogeneous catalysts can be heterogenized on carbon surface for increasing their efficiency. During heterogenization process, the uniformity between the molecules of catalyst (homogeneous) and the product is broken by converting them into two different phases[59]. This variation can be achieved by varying the polarity of two liquids or using one liquid component in combination with a solid. A homogeneous catalyst can be deposited on the surface of carbon support to achieve its heterogenization. Also, the surface functional groups of these carbon supports can be utilized to fabricate organometallic complexes with active metal centres. One such strategy is the attachment of carbene[60] with active metal centres to attain desirable activity. However, this strategy cannot be employed in metal-free catalytic reactions.

3.7 Composites

The carbon materials can be combined with other metal-free materials to target specific applications. The composites can be prepared either by combining one type of carbon material with another carbon material or it can be combined with other non-carbonaceous metal-free materials. The incorporation of two different carbon materials in a composite

system has already been proposed in literature as an efficient way to prepare highly efficient catalysts beyond the individual constituent carbon material[61]. There are numerous strategies that have been adopted to synthesize carbon-based composites which includes chemical vapor deposition (CVD)[62], hydrothermal synthesis[63], solution self-assembly process[64] and post-treatment of mixed-carbon materials with heteroatom containing organic precursor at high temperature[65]. Despite significant progress in this field, fabricating novel carbon-based composites using an innovative synthetic approach still remains a challenge.

3.8 Defects

The catalytic activity of carbon materials can be enhanced by incorporating defects in their perfectly crystalline structure. Doping with heteroatoms such as B, N, P and S to introduce external defects on the base surface of carbons has been shown to be a very effective strategy for increasing the adsorption capability of these carbon materials by changing the hybridization orbital type of carbon atoms[66,67]. The heteroatoms in carbon materials are commonly supposed to serve as active sites for various reactions because of external defects in them. However, researchers appear to negate the importance of intrinsic carbon defects, which are common in carbon materials. Intrinsic defects are frequently caused by changes in crystal lattice distortion or atom loss in these materials. These inherent defects can also modulate the electronic structure of material and surface properties, having a significant impact on rate of reaction under observation[68].

Herein, in this account, we are reporting such novel strategies to control the active sites in carbon-based materials for their applications in fine chemical synthesis and biomass conversion. Moreover, their use to design point-of-care units for developing portable devices for detecting the biochemicals in human serum is also presented.

4. Sensing probes and chemical transformations through metal-free carbon materials

4.1 Electrochemical Sensing

Carbon materials that show tendency to conduct electrons can be used for electrochemical sensing of different metal ions and important organic molecules in body fluids. One such important biomolecule found in human blood serum is a neurotransmitter called epinephrine (EP)[69]. Its flickering levels can cause various diseases including adrenal hyperplasia, hypoglycemia and chronic active hepatitis[70]. It is also used to medicate various allergic infections, glaucoma and emphysema[71]. Several analytical techniques such as high-pressure liquid chromatography, fluorimetry and capillary electrophoresis are reported for

the determination of EP levels in body fluids[72,73]. But most of the methods are not suitable for the analysis of biological samples due to acidic conditions[74]. However, electrochemical sensors are better suited for EP detection in this regard[75]. Various metal-based nanomaterials made up of iron[76], nickel[77] and gold[70] have been used for the electrochemical detection of EP. But such approaches for designing sensors for biological systems should be avoided because of their toxicity, high cost and restricted environmental reliability. As an alternative to this problem, carbon-based materials in addition to some modifiers have been employed for the electrochemical sensing of EP. There are several reports in literature on the use of multi-walled carbon nanotubes[78,79], graphene[80–82] and graphene quantum dots[83] for the electrochemical sensing of EP.

Carbon materials can be tuned properly for electrochemical sensing by modification of their structure, surface and conversion into different composites. Amino groups in electron rich melamine have been used with graphene oxide to create a metal-free composite (MGO) that possesses good current response and provides sites for the attachment of EP. The SEM and EDS analysis of MGO displayed a wrinkled surface along with granular-shaped structures on it that gave a clear-cut indication of the incorporation of melamine in between GO sheets[84]. The incorporation of N-rich melamine onto GO surface is confirmed from the highest percentage of N (31.8%) in MGO. The presence of $-NH_2$ groups was confirmed through deformation peak that appeared at 1605 cm^{-1} in the FTIR analysis spectrum[85]. Also, a decrease in the peak intensities of -OH and -C=O stretching confirmed the association of melamine onto GO surface leading to the formation of the $-CONH_2$ bond.

The cyclic voltammograms of bare GCE in the absence of EP along with bare GCE, MGO-GCE and GO-GCE were recorded in a 1 mM EP solution. The GCE was modified using GO and MGO which was used further for quantification of EP solution containing phosphate buffer at pH 7.2. The Ip_a of MGO-GCE (0.0533 mA) was greater than that of GCE and GO-GCE. The current response displayed by the MGO-GCE was 64.17 % higher than unmodified electrode. The CV results proved that MGO-GCE has excellent electrocatalytic properties for the detection of EP at physiological pH[86]. The pronounced and strong oxidation-reduction peaks of EP supported the hypothesis that MGO-GCE had higher electrocatalytic activity than GO-GCE. The electron transfer behaviour of melamine was explained by computational studies. A model molecule containing key active site (melamine) was chosen for examining its interactions with EP. The molecular electrostatic potential (MEP) calculations for melamine

(Figure 2a) molecule shows favourable positions for the nucleophilic and electrophilic attacks in the molecule. The high electron density region shown in red colour was favourable for the attack of electron-deficient species. These electron clouds encourage the attack of electrophiles and demonstrates the electron rich regions of melamine in the MEP image. The blue region of the electron cloud, in contrast, is electron-deficient and favours nucleophile attack. It also suggests that when the MGO electrode is connected to an external circuit, electron-rich regions in the melamine site help in the reduction of EP. Similarly, the electron-deficient region helps in the oxidation process. The limit of detection for melamine at the MGO-modified glassy carbon electrode was found to be 0.13 µM, indicating that the electrode could be used for biosensing of the neurotransmitter epinephrine. As a result, melamine incorporation creates a readily accessible electron donating and accepting centres on MGO-GCE electrode, assisting in the oxidation and reduction processes. Additionally, the -NH_2 group of melamine helps in the attachment of analyte on the electrode surface.

These properties of melamine were utilised properly after its attachment to another Janus 2D carbon material. Melamine and reduced graphene oxide (rGO) were covalently tagged on a highly ordered pyrolytic graphite (HOPG) resulting in the formation of Janus 2D carbon-based nanocomposite (JCC). This sensor was further utilized for the electrochemical detection of ascorbic acid (AA) due to its good redox characteristics[87,88]. The relationship between melamine and carbonyl group of rGO is confirmed by the FT-IR spectrum, where the appearance of peaks at 1400-1750 cm^{-1} and 3300-3500 cm^{-1} confirms the presence of amide functionalities in the JCC.

The CV spectra of bare rGO/HOPG along with JCC electrodes in $[Ru(NH_3)_6]^{2+/3+}$ / $[Fe(CN)_6]^{3-/4-}$ were taken in PBS buffer in presence and absence of 0.1 mM AA. A comparison of the Faradaic peak separation (ΔE_p) and peak current ratio $I_{o/r}=I_{ox}/I_{red}$ indicates that $[Fe(CN)_6]^{3-/4-}$ suits best for JCC electrodes. This is due to enhancement of surface chemistry, electroactivity, surface functionalities of JCC electrodes and kinetics of the reaction involved[89]. Furthermore, the analysis of specificity and sensitivity of JCC electrodes toward AA detection was carried out with the help of DPV study in presence of potential interferents dopamine (DA) and uric acid (UA). As a result, sturdy and distinct peaks of AA at 33 mV were seen for JCC electrodes in a mixture of interferents. The commercial use of

proposed sensor was demonstrated by fabricating a POC device (Figure 2b) integrated onto a polyimide (PI) substrate.

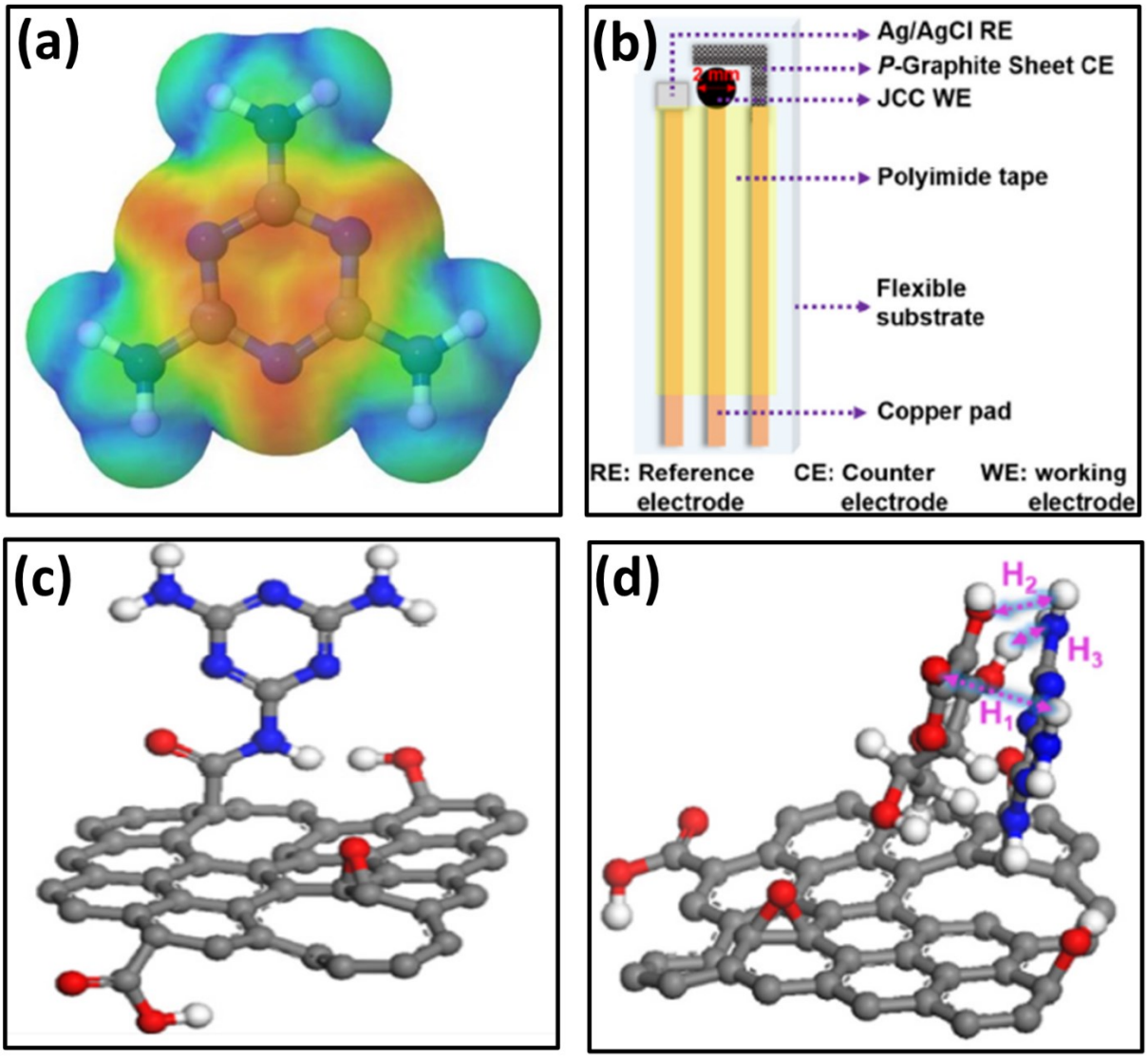

Figure 2. (a) Melamine MEP structure demonstrating the electron deficient region shown in blue colour and electron rich region shown in red colour (b)/(c) DFT optimized structure of JCC showing melamine at basal plane/AA molecule adsorbed on the JCC (d) Schematic representation of the POC device designed on a flexible substrate. Reprinted with permission from ref[86,87]. Copyright 2021 and 2022 Elsevier. All rights reserved.

It was then tested against AA in PBS buffer solution and a detection limit of up to 47 pM was reached, which overtook recently reported values[87]. Also, the sensing ability of this device was tested on real samples (serum, artificial sweat, artificial urine) and the device showed

excellent performance. The DFT studies were carried out to understand the interaction of proposed sensor with AA. The basal plane is preferred over the other, according to the free energy calculation of an amide-type bond formed at the basal or edge plane between melamine and rGO matrix of JCC (Figure 2c-d). The calculations show that AA adsorption takes place in a more stable conformation than DA adsorption, with relatively low free energy of formation and a shorter/stronger H-bonding distance. This thorough study clarifies the logical reasoning and fundamental physics developing the tuneable properties of Janus carbon-based organic sensors, clearing ways for the straightforward but efficient fabrication methods of biomolecule point-of-care devices.

Reduced graphene oxide (rGO) has garnered considerable interest for the fabrication of electrochemical sensors. Two highly efficient rGO catalysts (rGO-500/SPCE and rGO-600/SPCE) were prepared via electrospinning and calcination[90] methods. The effect of thermal annealing on electrochemical behaviour of these catalysts was also investigated. The prepared catalysts were further used for the electrochemical detection of neurotransmitter dopamine using screen printed electrodes (SPCEs) as reference electrode. The electrochemical behaviour of prepared catalysts towards detection of dopamine was studied via cyclic voltammetry (Figure 3) and differential pulse voltammetry (Figure 4). The cyclic voltammograms and differential pulse voltammograms of two catalysts were recorded in a 1 mM dopamine solution. A small peak current response towards DA was observed for bare/SPCE. On the other hand, the peak current response towards DA has shown a sharp increase by increase in concentration at both the electrodes. Similar behaviour was also seen for both the materials in DPV study. As a result of these findings, both the catalysts can significantly catalyse the oxidation process thereby leading to increase in rate of electron transfer in DA. The LOD of DA[90] as calculated from CV study was observed to be 1.11 µM and 1.23 µM for rGO-500/SPCE and rGO-600/SPCE respectively. On the other hand, LOD as obtained from DPV study was found to be 0.7 µM and 0.9 µM for rGO-500/SPCE and rGO-600/SPCE respectively. It can be inferred from the above findings that the DPV has elevated sensitivity in comparison to CV for the detection of DA.

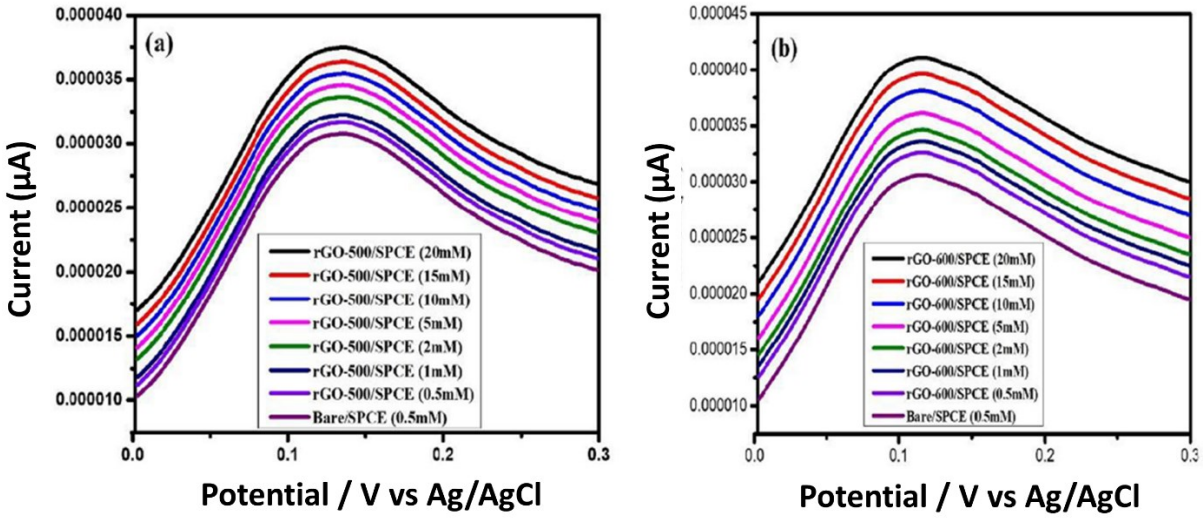

Figure 3. Cyclic voltammograms at different concentrations of DA (a) rGO-500/SPCE (b) rGO-600/SPCE. Reprinted with permission from ref[90]. Copyright 2022 Elsevier. All rights reserved.

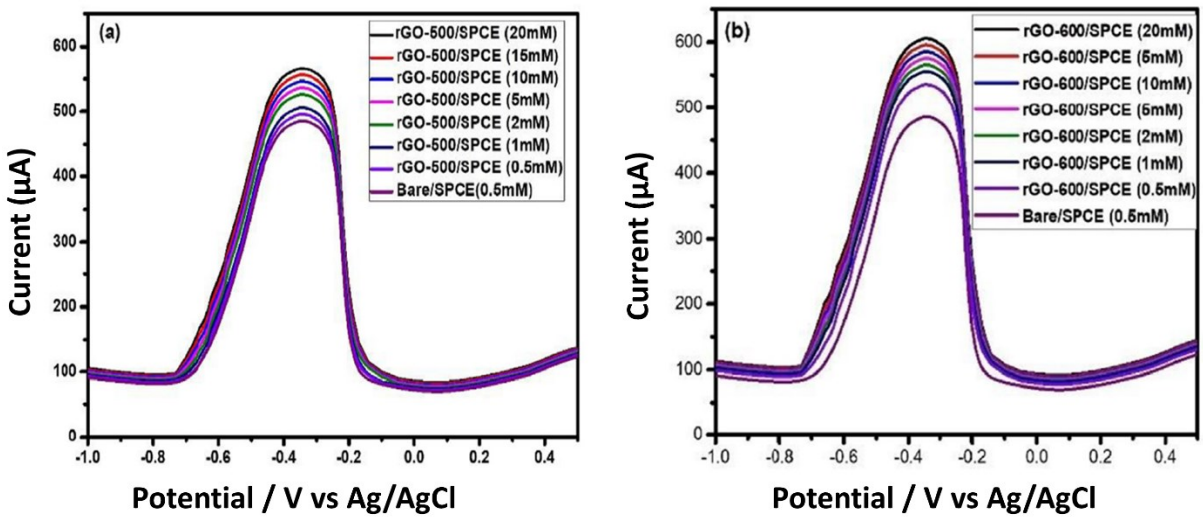

Figure 4. Differential pulse voltammograms at different concentrations of DA (a) rGO-500/SPCE (b) rGO-600/SPCE. Reprinted with permission from ref[90]. Copyright 2022 Elsevier. All rights reserved.

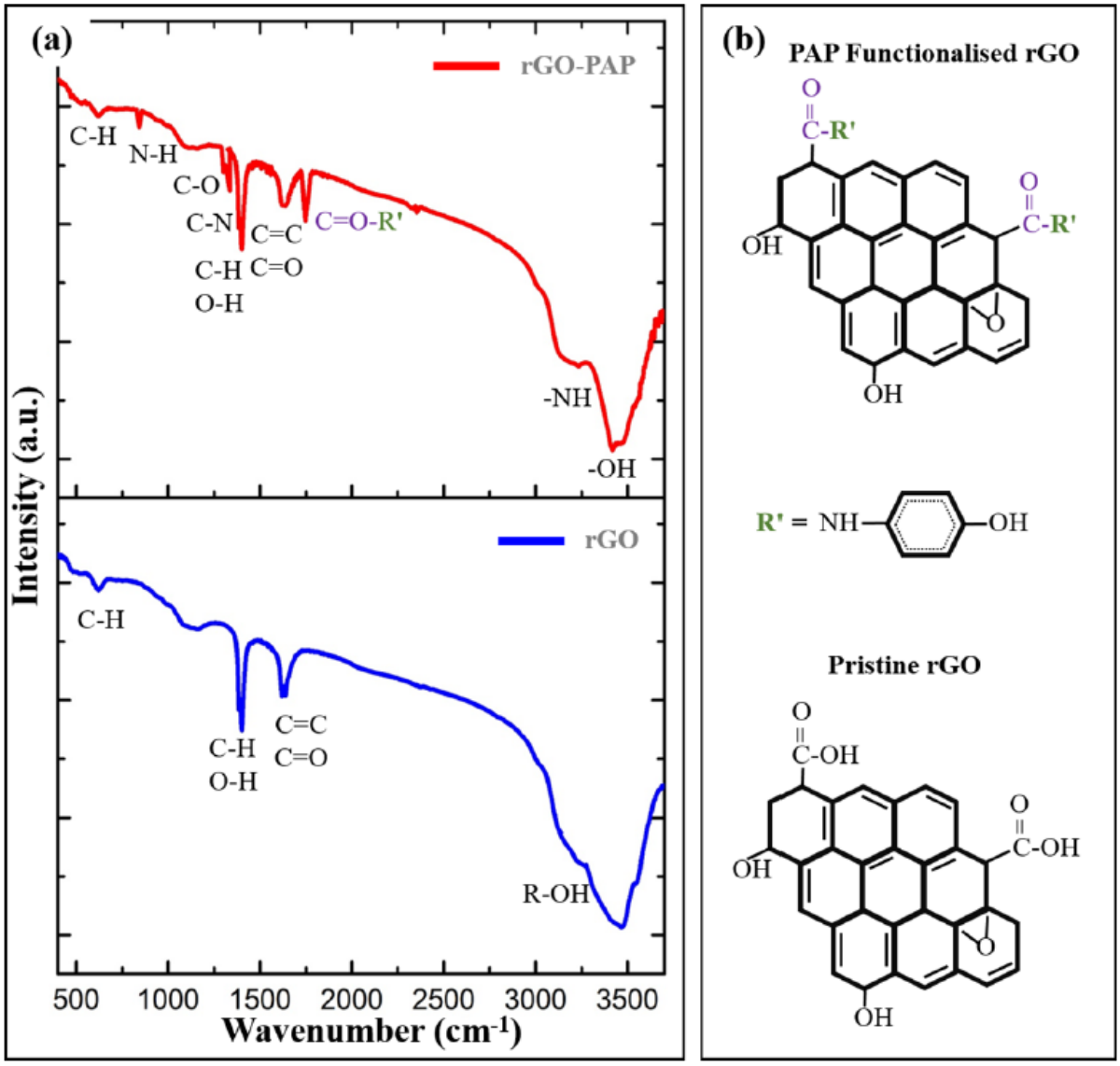

Figure 5. (a) The FT-IR spectra of the original rGO and the synthesised rGO-PAP showing a variety of peaks that have been attributed to the functional groups -OH, C=O, C=C, C-H, -N-C=O and C-O-C (b) Schematic representation of functional groups and bonding characteristics of the natural rGO and the synthesized rGO-PAP molecule. Reprinted with permission from ref[91]. Copyright 2021 American Chemical Society. All rights reserved.

Every material has different abilities to interact with the analyte and by evaluating the nature of the interaction, the performance of a material can be improved. A simple electron-rich molecule p-aminophenol (PAP) was grafted onto rGO via covalent linkage for this purpose. The TEM images of rGO-PAP nanostructures displayed wrinkled paper-like morphology that results from the reaction of rGO and PAP. A high amount of nitrogen (5.96%) on rGO surface confirmed that N-rich molecule was incorporated into its structure.

The covalent tagging of PAP molecule on rGO was confirmed by FTIR analysis (Figure 5), where the peaks of -OH, C=O, C=C, C-O-C and C-H were distinctly visible in rGO-PAP as well as pristine rGO[91]. Significant changes in the FTIR spectrum of rGO-PAP were seen in the region between 700–1750 cm^{-1} that showed the interaction of carbonyl groups of rGO with PAP molecule. New peaks at 850, 1320, 1340, 1740 and 3400 cm^{-1} corresponding to the N-H, -COO, C-N and R-OH were seen in the FT-IR spectrum of the rGO-PAP along with the pure rGO characteristic peaks. This confirmed that rGO-PAP contains hydroxyl, carbonyl and amide groups.

Utilizing cyclic voltammetry (CV) and differential pulse voltammetry (DPV), the electrochemical behaviour of the modified rGO-PAP electrode towards the oxidation of DA at various concentrations was investigated. Four distinct peaks in the CV curves of rGO-PAP modified electrode in presence of DA are governed by following reactions (Figure 6):

$$leucodopachrome \rightarrow dopachrome + 2H^+ + 2e^- \quad (1)$$

$$dopamine \rightarrow dopamine - o - quinone + 2H^+ + 2e^- \quad (2)$$

$$dopamine - o - quinone + 2H^+ + 2e^- \rightarrow dopamine \quad (3)$$

$$dopachrome + 2H^+ + 2e^- \rightarrow leuchodopachrome \quad (4)$$

Furthermore, the selectivity of the rGO-PAP modified electrode along with its cross-reactivity was investigated using common potential interferents uric acid (UA) and ascorbic acid (AA)[91,92]. It is very challenging to distinguish UA, AA and DA from each other in a mixture due to very close proximity of their oxidation peak potentials. The behaviour of bare GCE, pristine rGO and rGO-PAP modified electrodes was observed in a mixture of DA, UA and AA. The maximum value for current (21.4 A) was obtained at 0.25 V for the rGO-PAP electrode. This electrode provided single distinct peak for DA, whereas the bare GCE and pure rGO exhibit three and two broad anodic peaks, respectively. The concentration of AA and UA were 10 and 20 times greater than DA, respectively, throughout the entire study. These findings demonstrate that rGO-PAP has exceptional sensitivity and selectivity for detection of DA.

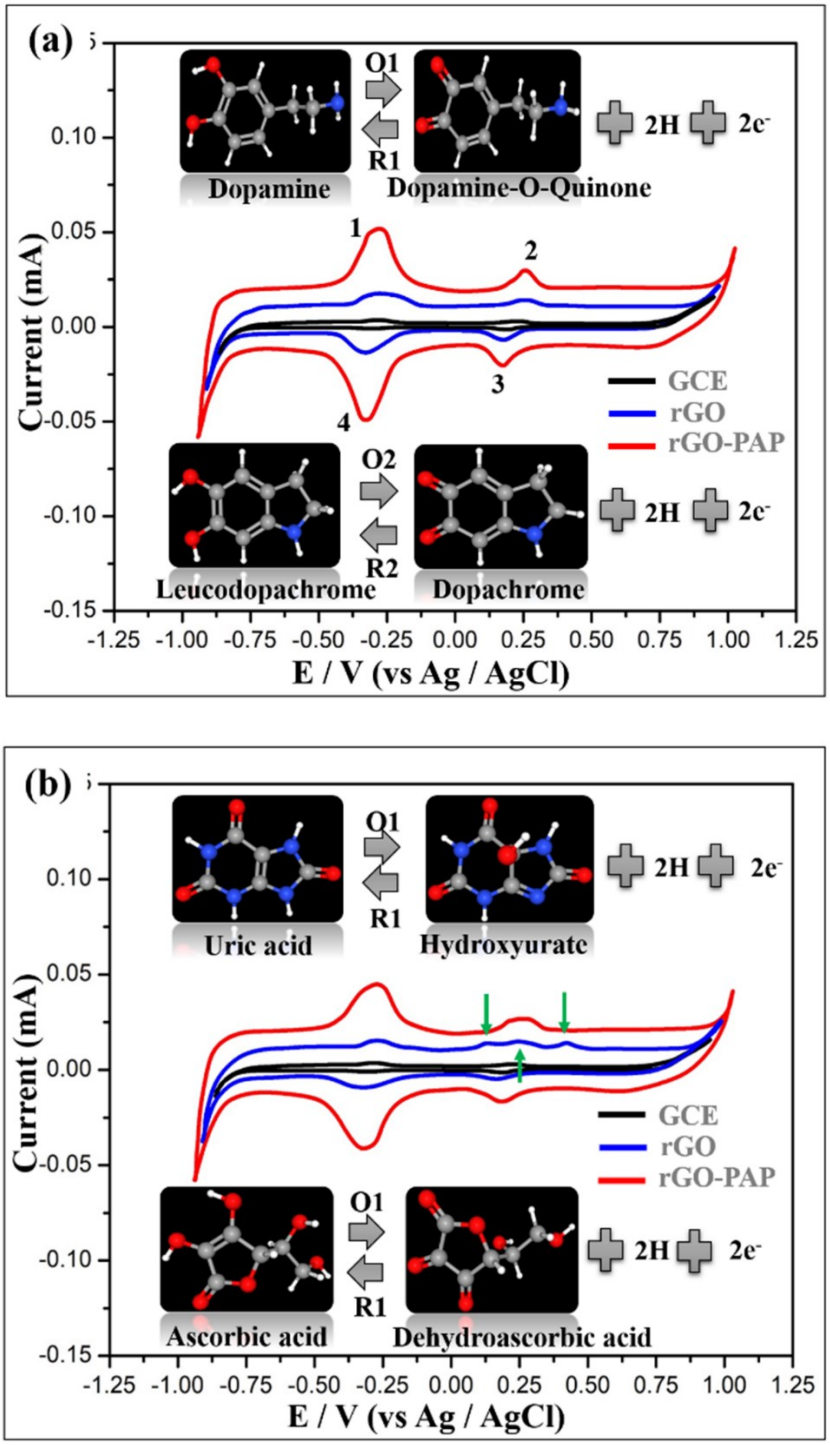

Figure 6. (a)/(b) Cyclic voltammograms of pristine, bare, and rGO-PAP-modified electrodes in presence of phosphate buffer solution (PBS) containing DA/DA + UA + AA. Insets show the mechanism of electrochemical reaction. Reprinted with permission from ref[91]. Copyright 2021 American Chemical Society. All rights reserved.

The LOD for rGO-PAP electrode was found to be 7.5 nM along with other interferents, which was lower than already reported metal-based and metal-free sensors[93]. The interaction of

rGO-PAP with DA via H-bonding was explained with the help of DFT computational study[93]. The terminal free -OH group in rGO-PAP electrode interacts via H-bonding selectively to the two -OH groups of DA rather than -NH_2 because the distance for an amine site is very large and interaction energy is lower than that of hydroxyl site. This strong H-bonding between rGO-PAP and DA lead to the sensitivity and selectivity of this electrode towards DA. The results show that by modifying the interface of rGO and other organic molecules, a reasonable, scalable and robust biosensor can be developed for the real-time analysis of body fluids.

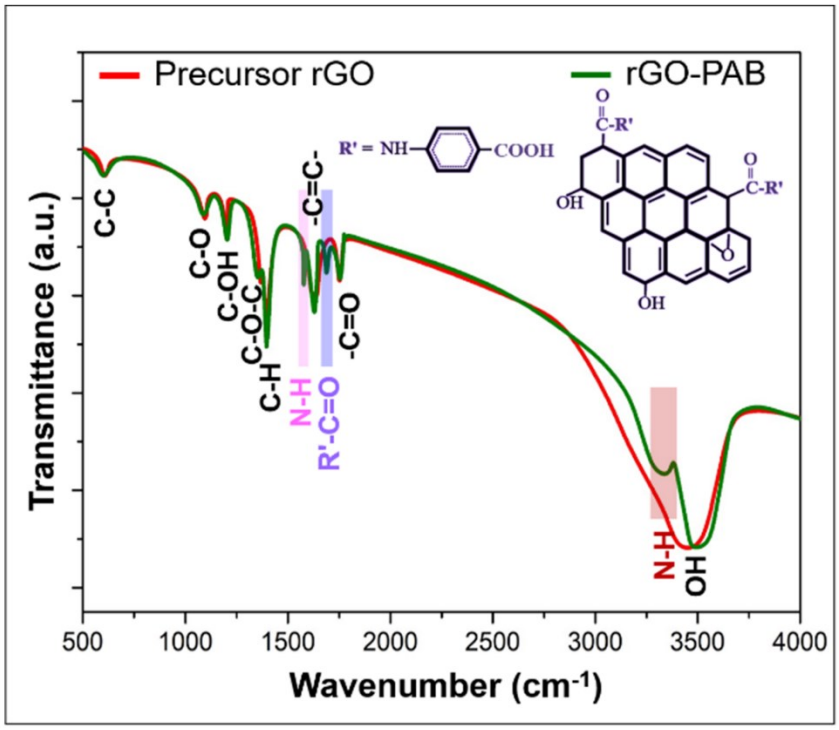

Figure 7. The FT-IR spectra of pristine rGO and rGO-PAB showing peaks of C=O,C-H, -N-C=O C=C, C-O-C, and -OH groups. Inset shows the schematic demonstration of the bonding nature as well as functional groups of rGO-PAB. Reprinted with permission from ref[88]. Copyright 2022 Elsevier. All rights reserved.

Not only PAP, but other organic molecules can also be used to enhance the sensitivity of these neuro sensors. In one such example, p-aminobenzoic acid (PAB) has been used to increase the sensitivity towards neurotransmitter EP down to picomolar (pM) levels[94,95]. The PAB molecule was anchored onto the basal plane of 2D-rGO resulting in a 3D-wrinkled porous nanostructures showing exceptional charge mobility, electron density, hydrophilicity and stability. The TEM images of rGO-PAB nanostructures displayed a 2D- wrinkled sheet-

like morphology, that is most likely formed by the reaction of rGO with PAB[88]. The FT-IR analysis of rGO-PAB (Figure 7) shows peaks of C=O, C-H, N-C=O, C=C, C-O-C, OH and NH groups[88]. The spectrum displays noticeable differences from pristine rGO due to generation of new structures after its interaction with PAB. This implies that during rGO functionalisation, PAB and the C=O of rGO are involved. The FT-IR spectrum of the rGO-PAB also shows characteristic peaks at 3300-3500 cm^{-1} and 1400-1750 cm^{-1} that corresponds to the N-H, NH-COO, C-N, and R-OH groups.

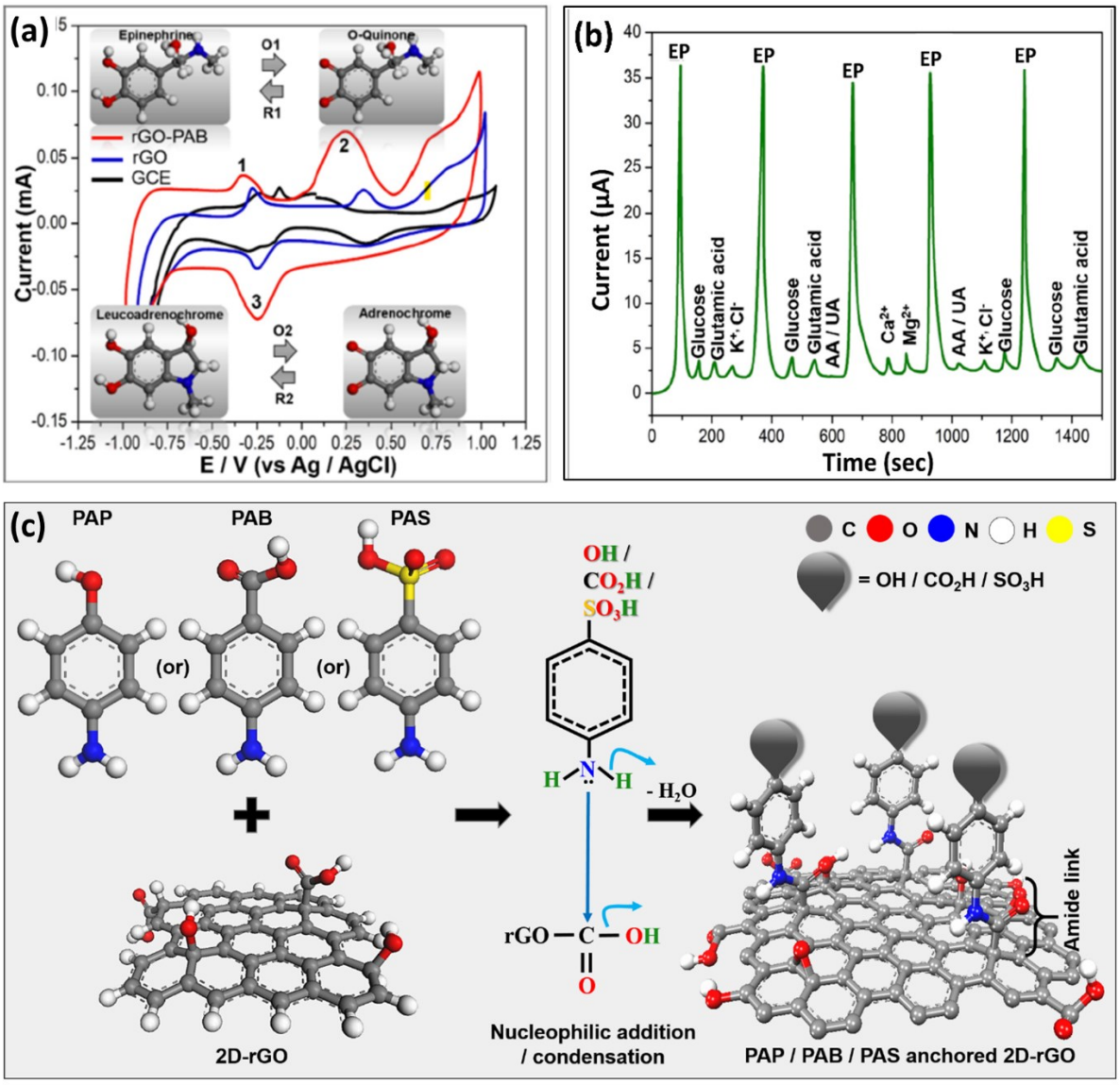

Figure 8. (a) Cyclic voltammograms of the GCE, pristine rGO, and rGO-PAB electrodes in phosphate buffer solution (PBS) containing 0.1 mM EP solution. Insets depict the mechanism of electrochemical redox reaction (b) Amperometry analysis of rGO-PAB specificity and electrocatalytic oxidation of EP (50 M) in PBS with equimolar concentrations

of AA, UA, KCl, glucose and glutamic acid (c) Schematic illustration of rGO-PAP/rGO-PAB/rGO-PAS formation by reaction with -NH_2 functionalized aromatic molecules. Reprinted with permission from ref[88,96]. Copyright 2022 Elsevier and Wiley. All rights reserved.

The CV curves of pristine rGO, rGO-PAB and bare GCE are recorded in the presence and absence of EP in PBS buffer solution (Figure 8a). No significant redox peaks are observed for the bare GCE and pristine rGO, while rGO-PAB modified electrode exhibits significant redox peaks with anodic peak (E_{pa}) at 0.24 V with a current response of 74 µA. Furthermore, the specificity of rGO-PAB towards EP in presence of KCl, AA, UA, glutamic acid and glucose in PBS buffer at a potential of +0.232 V was checked via amperometry technique (Figure 8b). Addition of equimolar quantities of these interfering agents does not results in any significant decrease in the current response. The additions of AA and UA, in particular, have no effect on the current intensity of rGO-PAB electrode. This result was in agreement with the CV study and confirm the remarkable specificity of rGO-PAB material for EP detection. Also, the commercial application of the sensor is provided by designing a portable POC device that was developed on the same pattern as reported in Figure 2b. The device was tested against EP in real serum samples. It is observed that the detection limit of the fabricated sensor for EP detection was as low as 20 pM. The wide linear range and lower LOD of this POC sensor has proved its potential for practical applications.

Another highly efficient organic carbon-based sensor was designed to be used as a POC device for the detection of DA. The physicochemical characteristics of the material were tuned accordingly via one-step molecular engineering (ME) process. In this approach, three aryl amine derivatives [p-aminobenzoic acid (PAB), p-amino sulphonic acid (PAS) and p-aminophenol (PAP)] containing two nucleophilic sites at both ends were immobilized onto the surface of rGO (Figure 8c). The covalent anchoring of organic moieties in addition to mild reduction of oxide functional groups in the matrix of rGO host enabled the distribution of electrons within the matrix. The HR-TEM images of rGO-PAB/rGO-PAS/rGO-PAP nanostructures[96] displayed a 3D creased-sheet-like topology which mostly results from the interaction of rGO and anchoring molecules during molecular engineering[97]. FT-IR was used to investigate the bonding nature and surface functionalities of as-synthesized samples. The FT-IR spectrum displayed peaks of the C-O-C, NH, C-O, C-H, C-C, N-C-O, OH and SO groups in the rGO-PAS/rGO-PAP/rGO-PAB samples. Due to the development of novel structures,

significant variations between the relevant samples along with unaltered and functionalized rGO spectra were seen. It is proved that throughout the ME process, there occurs interaction of the anchoring molecules to C=O group of the rGO[97].

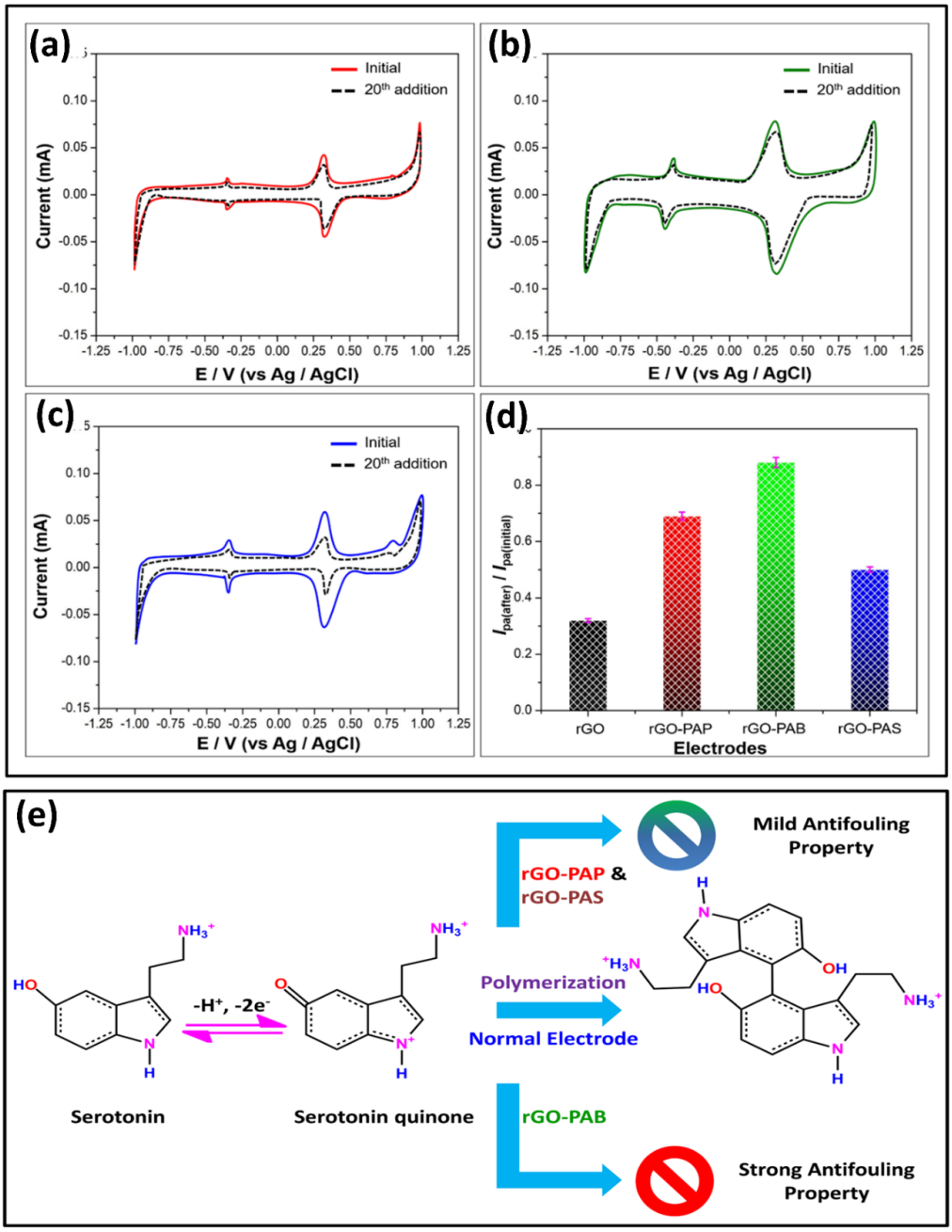

Figure 9. Serotonin (5-HT) biomolecule-based electrochemical fouling study. (a)/(b)/(c) CV curves at rGO-PAP/rGO-PAB/rGO-PAS after the first (solid) and twentieth (dashed) additions of $1x10^{-6}$ m 5-HT. (d) Ipa or normalised anodic peak current values for various sensors (e) Schematic representation of serotonin polymerization-induced electrode fouling. Modified and reproduced with permission from ref[96]. Copyright 2022 Wiley. All rights reserved.

The CV curves of GCE, pristine rGO, and rGO–PAS/rGO–PAP/rGO–PAB electrodes were recorded in the presence of 100 × 10^{-6} M solution of DA. The sensitivity, specificity and analytical capability of sensing materials for DA detection were investigated using the DPV technique. The oxidation of DA provided prominent peaks for rGO-PAP/rGO-PAB/rGO-PAS, whereas the GCE and pure rGO electrodes exhibit no discernible signals[97]. Finally, a POC device integrated with polyethylene terephthalate (PET) was designed on the same pattern as reported in Figure 2b for proving the flexibility, simplicity and commercial application of synthesized biosensor. The constructed POC device allowed the detection of DA up to 10 x 10^{-12} M level in the physiologically complicated serum sample. Aside from serum, other physiologically complicated samples (artificial sweat and urine) were also used to test the sensing ability of fabricated POC device. It was observed that the fabricated sensor can detect DA as low as 40 x 10^{-9} M in urine and 20 x 10^{-9} M in artificial sweat samples.

The actual molecular interaction between sensor and dopamine were verified by DFT studies. Comparing other covalent linkages such as ester linkage/basal-edge plane or amide linkage/edge plane sites, it was observed that the amide linkage between the organic molecule and the basal plane structure is selectively preferable. The planar structure is changed by the resonance effect and covalent interaction due to an increase in electron density or delocalization. Electrode fouling while in use is one of the main drawbacks of a biosensor because it reduces its response as several electroactive species are formed on its surface. Thus, the electrode fouling of a neurotransmitter serotonin (5-HT) during electrochemical reactions was investigated in this regard. The fabricated sensors (rGO-PAS/rGO-PAP/rGO-PAB) were exposed to serotonin solution (1*10^{-6} M) and the Ip_a for these electrodes was measured at a periodic interval of every 5 seconds (Figure 9). When serotonin is electrochemically oxidised, it produces serotonin quinone radical species which polymerizes and reduces the electroactive surface area. Figure 9e shows a schematic representation of the serotonin polymerization-induced electrode fouling process. The normalised Ip_a of rGO-PAB (Figure 9d) is greater than pristine rGO, rGO-PAP and rGO-PAS sensors, all of which have exceptional antifouling properties. These findings show that using a ME with the appropriate organic moiety can help to reduce electrode fouling. This thorough investigation clarifies the underlying logic and fundamental physics that underlie the adaptable characteristics of carbon-based sensors, opening the doors for the development of point-of-care devices for neurotransmitters detection.

4.2 Biomass Valorisation

The chemical industry continues to rely heavily on conveniently accessible and reasonably priced petroleum-based carbon feedstock. In the near future, there will be a significant change in the utilization of feedstock due to rising crude oil costs, the effects of climate change and declining oil reserves. The future of the chemical industry will heavily rely on the production of fine chemicals and materials from renewable feedstock, including waste. This is also true for the production of energy, where renewable resources play a major role[98]. Burning fossil fuels is the most widely used method of producing energy worldwide. It produces toxic pollutants such as carbon dioxide (CO_2), which is the primary factor causing greenhouse effect, as well as other gases including sulfur oxide (SO_x), carbon monoxide (CO), nitrogen oxide (NO_x) and methane (CH_4). The intensive use of fossil fuels has resulted in environmental degradation, which has prompted the quest for alternate energy sources[99]. On the other hand, there is continual pressure towards transition from a petrol-based economy to a sustainable one due to factors including climate change[100], overexploitation or depletion of traditional sources[101] and rising pollution levels[102]. In order to alleviate this, numerous renewable energy sources (such as wind, solar, etc.) are now being researched and put into practice[103]. However, there are limited sustainable possibilities available for producing chemicals and biomass valorization[104] is a powerful alternate in this regard.

Biomass valorization[105] focuses on adding value to various plant products and residues including food crops, rice husk, corn husk, aquatic plants (algae), lignocellulosic plants, municipal waste. Among all of these, using food crops for producing value added chemicals and products can be avoided because they are produced for use by humans and animals. This is especially true considering the fact that the world's population will reach more than 9 billion by the year 2050[106]. In reality, greater population density will result in greater use of energy and chemicals as well as fewer food sources being available. In light of this development, lignocellulosic plants are preferred for the manufacture of plastics, medications and other chemicals because they contain a variety of components that can be valorized for a variety of applications. These plants are made up of cellulose, hemicellulose, and lignin[107]. Despite the difficulty of converting lignin into a desired product[108], cellulose and hemicellulose can be converted into important biobased platform chemicals with or

without pre-treatment[109]. The creation of effective and long-lasting catalytic processes is of utmost significance in this direction that falls within the framework of the circular (bio)economy. Designing new catalysts is very important in this context where metal-free carbon-based nano-catalysts can act as one of the most promising classes of materials for biomass valorization.

In this regard, two nitrogen-rich carbon nanotubes (NCNTs) were synthesized by a chemical vapor deposition (CVD) technique and subsequently utilized as metal-free catalyst for the conversion of glycerol into dihydroxyacetone (DHA) using tert-butyl hydroperoxide as an oxidant. Both catalysts were tested for selective oxidation of glycerol. The selectivity and activity of commercial CNTs (CNT_{comm}) along with commercial nitrogen-doped CNTs ($NCNT_{comm}$) were also compared with the prepared catalysts. It was observed that unfunctionalized CNTs were found almost inactive for the oxidation of glycerol. On the other hand, conversion of 36.5%, 8.3% and 15.3% was observed for NCNT700, NCNT800 and $NCNT_{comm}$ respectively after 6h reaction time. Atomic Absorption Spectrometry results have shown the presence of 0.3% and 0.1 % of Fe for CNT_{comm} and $NCNT_{comm}$ respectively. However, CNT_{comm} were almost inactive for oxidising glycerol which confirmed that the Fe impurities encased inside CNTs are inaccessible to the reactant[110]. The activities of prepared catalysts were compared with their surface properties. It was observed that NCNT700 was the most active catalyst containing the highest amount of pyridinic groups (13.4%) in comparison to NCNTcomm (3.8 %), NCNT800 (1.9 %), and CNTs (0.1 %). The electronic structure of the nearby carbon atoms is altered by the presence of graphitic nitrogen, which increases the catalytic performance in alcohol oxidation[110,111]. Additionally, a strong correlation was observed between pyridinic nitrogen and the activity of N-functionalized carbon in the oxidation of alcohol[110,112]. The reaction barriers were calculated using quantum chemical calculations and proposed a pathway in order to look into the preferred synthesis of DHA by NCNT700 (Figure 10). To explore the reactivity of primary and secondary hydroxyl groups, propane-1,2-diol was chosen as the model substrate.

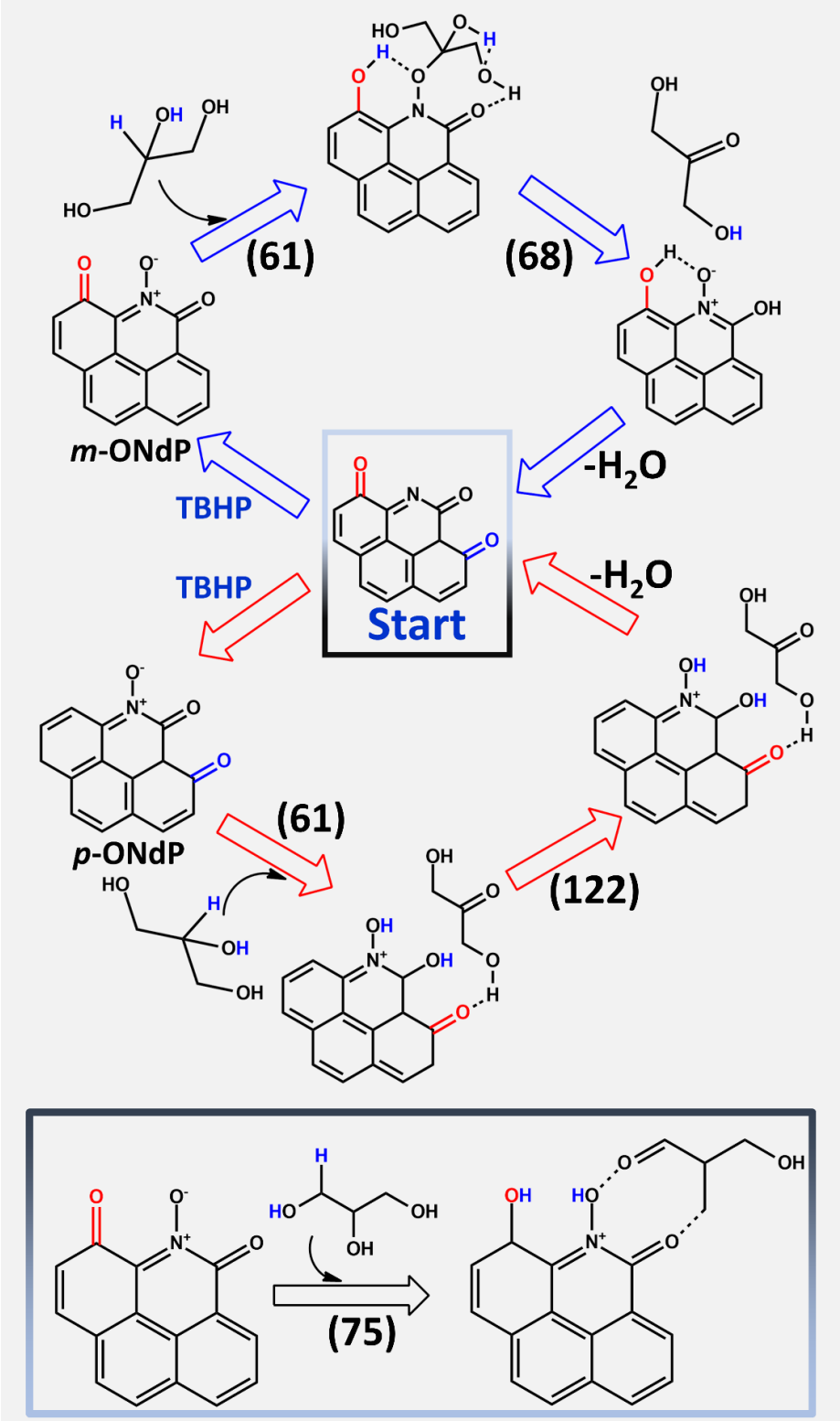

Figure 10. Mechanism proposed for the conversion of glycerol into dihydroxyacetone (DHA). The predicted quantum-chemical reaction energy barriers are listed in parentheses (in $kJmol^{-1}$) for the oxidation of propane-1,2-diol. Modified and redrawn with permission from ref[110]. Copyright 2017 Wiley. All rights reserved.

It was proposed that pyridinic N rich-CNTs were the active sites for selectively oxidising glycerol into DHA. This encouraged that pyridine-N-oxide, pyridine oxime and quinone groups adjacent to N sites promotes this oxidative conversion. The first proof of concept for this reaction has been presented by covalent tagging of 2,4-dihydroxypyridine (DHP) to GO surface[30]. The carbon atom next to the N centre (C=O) was already oxidized in this molecule and it incorporated in the active site on GO surface. The tautomer of this molecule resembled proposed reactive sites within the carbon cluster. Therefore, the GO catalyst surface was tagged with this molecule through an ester bond (Figure 11).

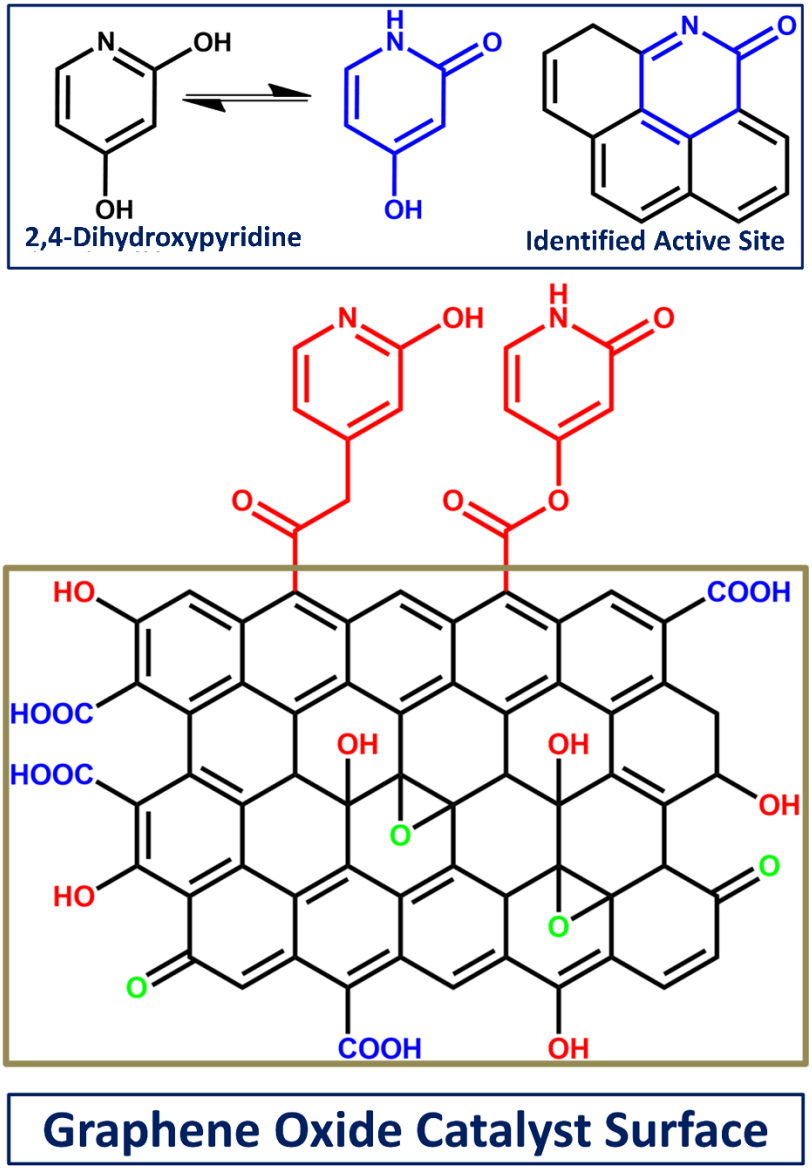

Figure 11. 2,4-dihydroxypyridine (DHP) functionalized graphene oxide catalyst. Modified and redrawn with permission from ref[30]. Copyright 2021 Royal Society of Chemistry. All rights reserved.

FTIR spectroscopy was used to confirm the presence of functional groups on the surface of DHP@GO. The prepared material was then used in catalytic glycerol oxidation (Scheme 1).

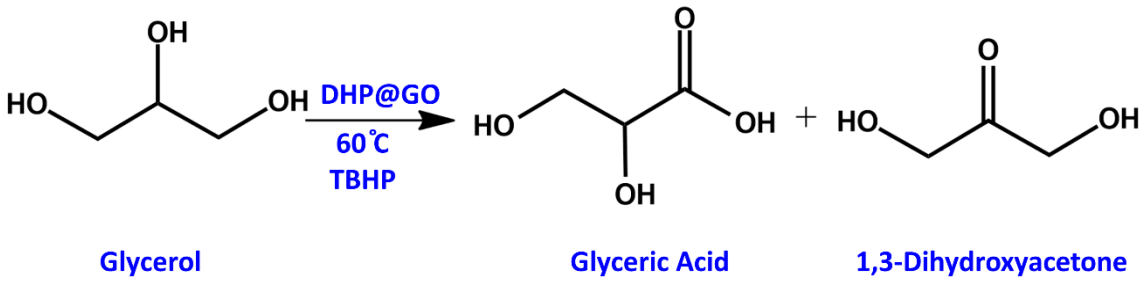

Scheme 1. Metal-free oxidation of glycerol in the presence of DHP@GO as a catalyst. Modified and redrawn with permission from ref[30]. Copyright 2021 Royal Society of Chemistry. All rights reserved.

As anticipated, DHP@GO accelerated glycerol conversion into dihydroxyacetone (major product) along with minute quantities of formic and glyceric acid. Additionally, the transition from pure GO to DHP@GO greatly boosted conversion as well as selectivity toward DHA. This work has thus paved the way for the development of more efficient carbon-based catalysts with restricted quinone sites next to N atoms for improved glycerol conversion and selective oxidation.

Over the coming decades, biomass will be utilized extensively in the synthesis of chemicals[113]. It implies that producing billions of tonnes of chemicals derived from biomass will be necessary. Heterogeneous catalysis will face a significant obstacle in achieving this goal because it must shift its emphasis from the well-known C-C bond chemistry to C-O bond chemistry. Basic heterogeneous catalysts will be crucial in this scenario for reactions[113–115] such as hydrolysis, aldol condensation, dehydration, (trans)esterification, hydrolysis, isomerization or alkylation. At present, the most common types of basic heterogeneous catalysts[113,116] are clays, modified zeolites, alkaline oxides and alkaline-earth oxides. They have a variety of limitations, including a dearth of accessible active sites, significant diffusion and mass transfer issues along with partial dispersion in the reaction medium for use in liquid-phase reactions[113,117]. Therefore, it is essential to create new, fundamental heterogeneous catalysts that are higher selectivity and stability that are simple to modify both on nano- as well as macro-scale. Multiwalled carbon nanotubes (MWCNTs) based catalysts are found to be appropriate for this purpose.

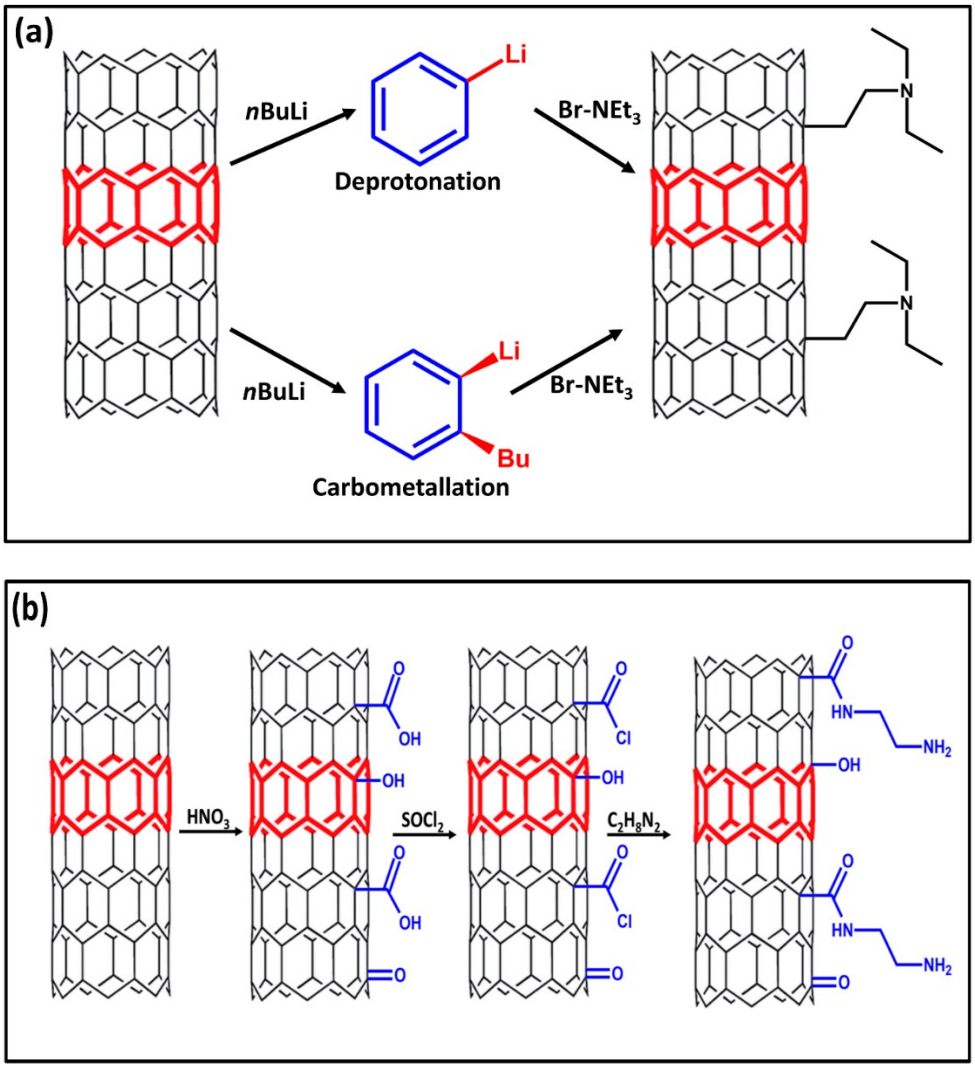

Figure 12. (a) Functionalization of MWCNTs by deprotonation–carbometallation involving simultaneous attack of the bromotriethylamine. (b) Conventional oxidation-amidation method for functionalization of MWCNTs. Modified and redrawn with permission from ref[118]. Copyright 2009 Angewandte Chemie. All rights reserved.

In this regard, MWCNTs-grafted amino groups were prepared by a facile and novel method that has been further used as catalyst for biomass valorisation. The catalysts were prepared by a grafting technique (Figure 12 a), where MWCNTs were reacted initially with an excess of *n*BuLi that lead to the deprotonation of C-H bonds near defects and replacing them with C-Li bonds. Also, *n*BuLi effected the carbometallation of MWCNTs. Afterwards, 2-diethylaminoethylbromide was added to the activated MWCNTs, which resulted in an electrophilic attack on C-Li bond. As a result, the formation of a new C-C bond between the amine's ethyl group and the MWCNTs initiates the covalent functionalization of the nanotube with triethylamine and the subsequent production of LiBr. Another sample was

also used for comparison that was prepared by the traditional oxidation-amidation route (Figure 12 b).

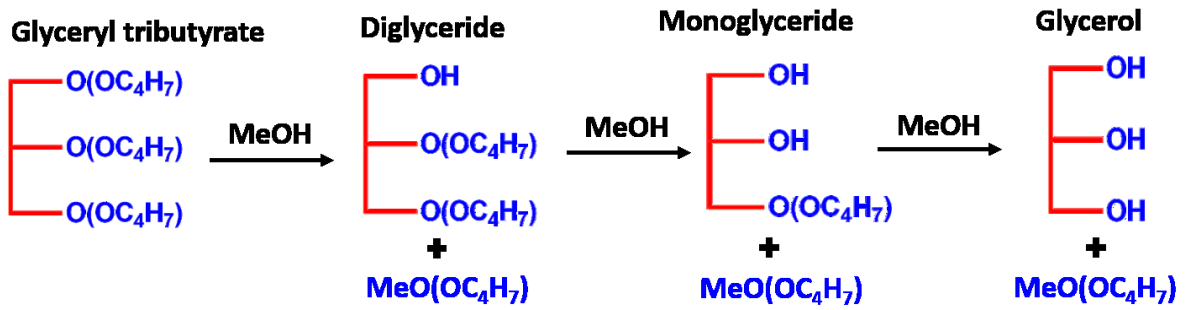

Scheme 2. Transesterification of glyceryl tributyrate to methyl butyrate in presence of methanol.

The energy-dispersive X-ray spectroscopy (EDX) confirmed the presence of N in both samples. However, it was discovered that the sample made using the proposed electrophilic attack method had a lower nitrogen peak than the sample made using oxidation-amidation[118]. Additionally, when compared to the sample prepared using the suggested electrophilic method, the Raman spectrum of the sample prepared using the conventional oxidation-amidation method showed relatively wider peaks with a slightly higher D/G ratio. These additional defects are believed to be created most probably during oxidation using nitric acid. The two samples were then tested for biomass conversion reactions as a potential heterogeneous catalyst. Their ability to catalyze the transesterification of glyceryl tributyrate with methanol, a test reaction for the synthesis of biodiesel, was investigated (Scheme 2)[119]. The obtained results were then compared with the commercial hydrotalcite used as a standard catalyst (Figure 13)[119]. The target ester methyl butanoate was consistently found to be the major product, and the diglyceride and monoglyceride reaction intermediates made up less than a few percent of it. After 8 hours, the catalyst synthesized using proposed method achieved a conversion of 77%. On the contrary, the hydrotalcite tested under identical conditions achieved a conversion of 51 % only.

The sample prepared by oxidation-amidation seemed to have the lowest conversion. Although the grafted amino groups are sufficiently basic to catalyse the transesterification reaction, the activity and deactivation of this catalyst were unsatisfactory. Both bases and acids can catalyze transesterification reactions. However, acid-base titration has shown that

the neighboring basic amino groups and the remaining acidic oxygen-containing groups in the sample can neutralize each other. As a result, there are lesser active sites accessible to catalyze the transesterification process which explains the decreased rate of triglyceride conversion[118]. These results reveals that the catalytic activity of as-prepared catalysts has significantly enhanced via covalent grafting of amino groups on its surface.

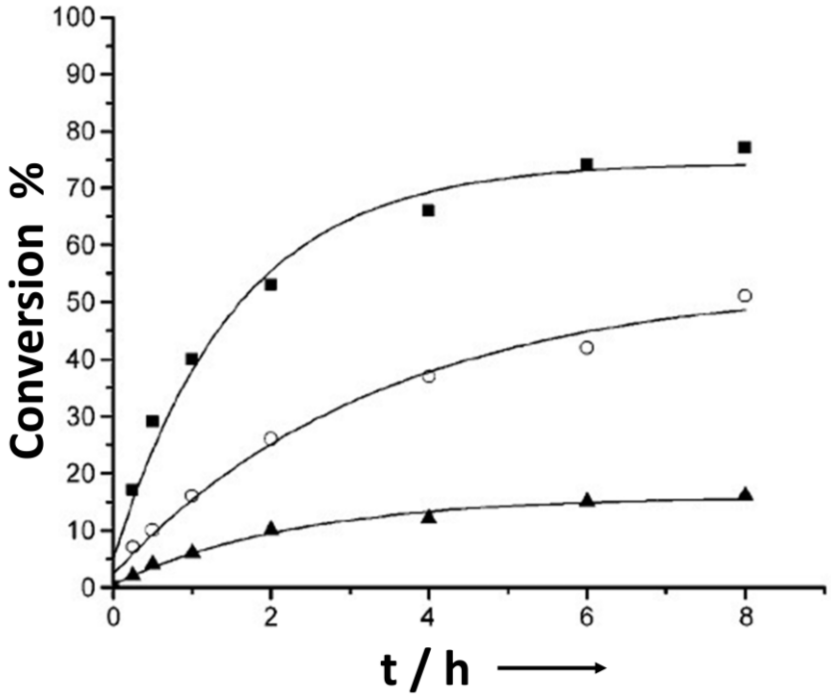

Figure 13. Triglyceride conversion as a time-varying variable measured for samples prepared by common oxidation-amidation route (▲NH_2-MWCNT), electrophilic attack (■ NEt_3-MWCNT) and for commercial hydrotalcite (○). Reprinted with permission from ref[118]. Copyright 2009 Angewandte Chemie. All rights reserved.

In contrast to conventional CNTs, nitrogen-doped CNTs (N-CNTs) have enhanced physico-chemical properties due to the incorporation of defects and nitrogen groups in their basal planes. Herein, a new methodology has been reported for the preparation of amino-functionalized CNTs that have been used as a basic catalyst for the transesterification of triglycerides. Three different catalysts were prepared by grafting various amines such as ethylamine, triethylamine and pyrrolidine onto the CNT surface. They are denoted as $EtNH_2$-CNT, Et_3N-CNT and C_4H_9N-CNT respectively. Acid-base titrations as well as TG-MS measurements were carried out to investigate the thermal stability and quantification of the anchored groups. The TG-MS data demonstrate the stability of the catalysts at a

temperature greater than the boiling point of corresponding amines, explaining that the amino groups were anchored on the CNTs successfully[120].

The catalytic activity of as-prepared amino-grafted CNTs was examined for the transesterification of glyceryl tributyrate at 60 ^{0}C. Et_3N-CNTs were found to be the most active catalyst with a conversion rate of 77% after 8 h (Figure 14). The C_4H_9N-CNTs exhibited a substantially lower conversion and $EtNH_2$-CNTs catalyst achieves a conversion of 55% under identical reaction conditions. The differing catalytic capabilities of Et_3N-CNTs and $EtNH_2$-CNTs can be attributed to the varying pK_a values of grafted amines. The decrease in the number of grafted pyrrolidine groups may be caused by different reactivity of 1-(2-chloroethyl) pyrrolidine hydrochloride as compared to Bromo derivatives that were utilized to graft the other two amines.

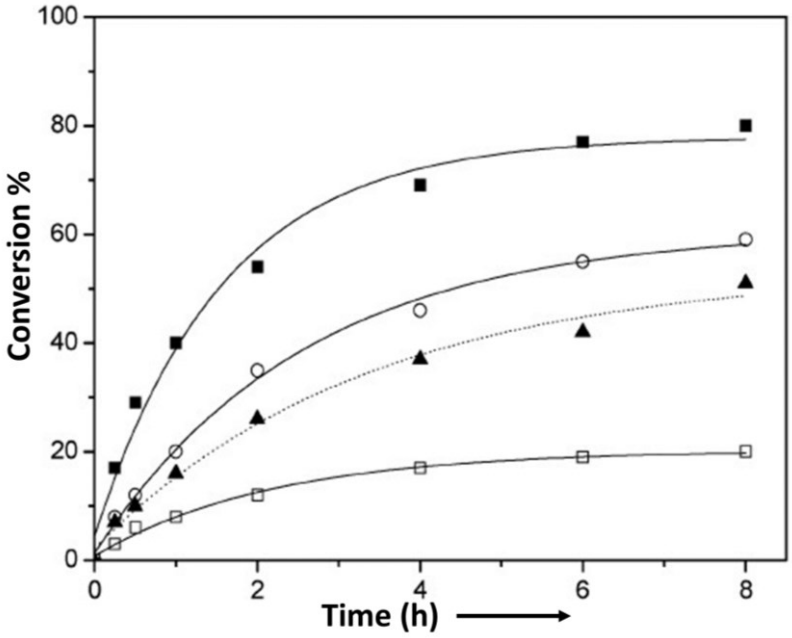

Figure 14. The effect of different amines implanted on CNTs in glyceryl tributyrate transesterification: (■) Et_3N-CNTs, (○) $EtNH_2$-CNTs, (▲) hydrotalcite, (□) C_4H_9N-CNTs. Reprinted with permission from ref[120]. Copyright 2009 Royal Society of Chemistry. All rights reserved.

Additionally, a comparison of the activity of amino-grafted CNTs was performed with a commercial hydrotalcite catalyst. While hydrotalcite showed conversions of 51% after 8 hours, Et_3N-CNTs and $EtNH_2$-CNTs demonstrated superior catalytic efficacy with conversions of 77 and 55% respectively. Therefore, the grafting of amino groups onto CNTs is an

appropriate way to produce active and reliable basic catalysts for use in liquid-phase processes.

It has previously been explained that the methodology for grafting N-containing functionalities onto surface of multi-walled carbon nanotubes (MWCNTs) has a significant impact on the catalytic activity of N-CNTs[118,120]. Three nitrogen-doped CNTs (Et_3N-CNTs 1, Et_3N-CNTs 2 and Et_3N-CNTs 3)[118] were synthesized by following a previously published procedure. The prepared catalysts were successfully tested for the transesterification of glyceryl tributyrate[29]. It was observed that the catalyst with higher concentration of basic moieties (Et_3N-CNTs 3) has shown excellent activity as compared to Et_3N-CNTs 1 that was eventually deactivated. Furthermore, the catalytic activity of the prepared catalyst[29] was enhanced significantly at elevated temperatures and higher methanol to glyceryl tributyrate ratios.

According to research reports, phosphorylated carbons are believed to act as efficient and effective catalysts in the dehydration reactions during biomass valorization. One important factor influencing the catalytic performance of these functionalized materials is the quantity and nature of P groups. In this study, the structural and surface characteristics of several carbon nanofibers affecting the quantity of P-functionalities along with their catalytic performance have been investigated. Phosphorus-rich carbon nanofibers (CNFs) with varying degrees of graphitization have been prepared by treating them with H_3PO_4 - HNO_3 mixture at 150 ^{0}C temperature. The catalytic performance of this material has been accessed through selective dehydration of fructose to hydroxymethylfurfural (HMF) (Scheme 3). The activities of samples reporting the conversion of fructose as a function of reaction time have been compared in Figure 15. To provide a point of comparison, pure materials, Low-temperature Heat Treated Carbon Nanofibers (LHT-CNFs), Pyrolytically Striped Carbon Nanofibers (PS-CNFs) and High-temperature Heat Treated Carbon Nanofibers (HHT-CNFs) were also examined with very little (2% fructose conversion in all cases). Phosphorus functionalized High-temperature Heat Treated Carbon Nanofibers (P-HHT CNFs) demonstrated the highest levels of activity among the materials under study, converting 94% of fructose in 12 hours. The other two samples, Phosphorus functionalized Pyrolytically Striped Carbon Nanofibers (P-PS) and Phosphorus functionalized Low-temperature Heat Treated Carbon Nanofibers (P-LHT) displayed lower conversion rates

(17% and 20%, respectively). Moreover, the two catalysts also showed signs of deactivation after 3 hours.

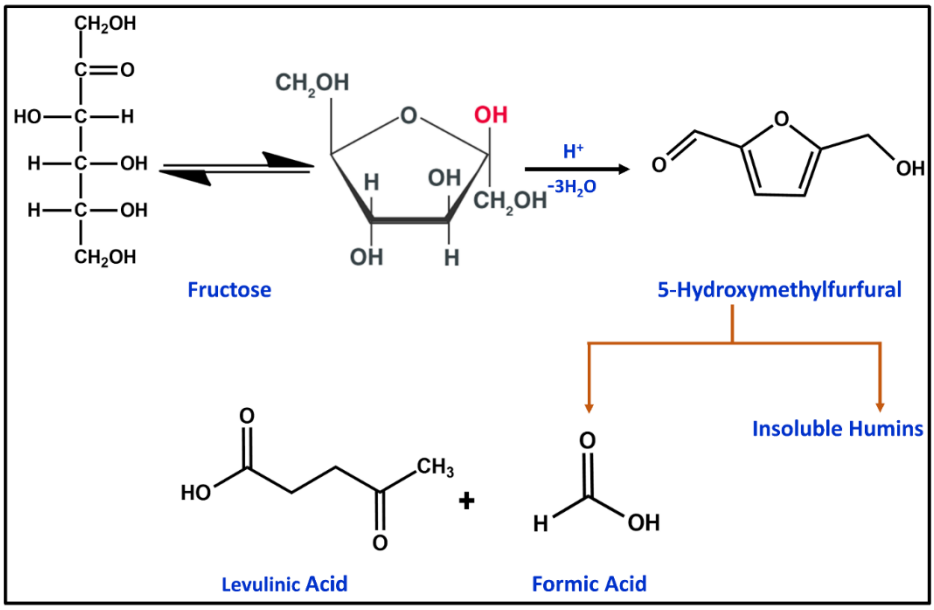

Scheme 3. Schematic demonstration of fructose dehydration. Modified and reproduced from ref[121]. Copyright 2018 C-Journal of Carbon Research. All rights reserved.

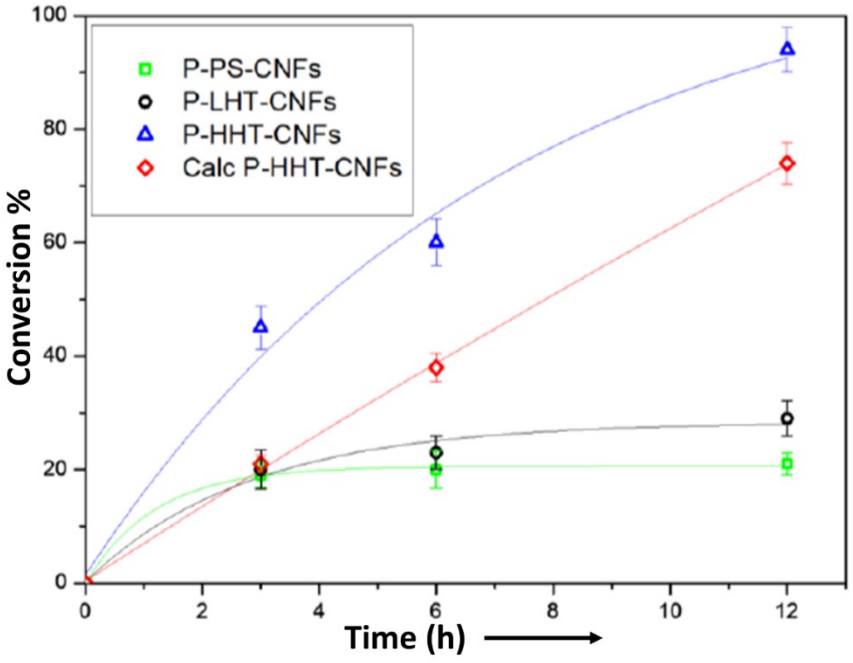

Figure 15. Catalytic activity of prepared samples governing conversion of fructose as a function of the reaction time; (fructose/catalyst 2:1 w/w, fructose 5 wt % in water, $p(N_2)$ = 3 atm and T = 120 ^{0}C). Modified and reproduced from ref[121]. Copyright 2018 C-Journal of Carbon Research. All rights reserved.

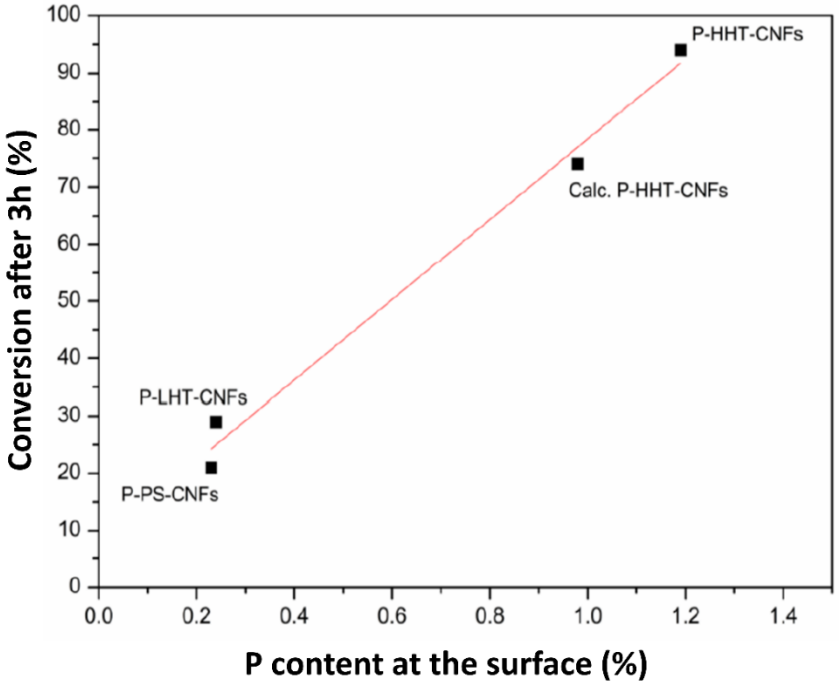

Figure 16. Correlation between activity of the V and amount of P content present on catalyst surface. Modified and reproduced from ref[121]. Copyright 2018 C-Journal of Carbon Research. All rights reserved.

The relative concentration of P functional groups on the surface of CNFs and the extent of functionalization affects their catalytic performance in fructose dehydration. The dehydration of fructose selectively to HMF is catalyzed by acids. Brønsted acid sites particularly the phosphate groups are recognized as effective catalytic sites for this reaction[122–125]. In fact, a strong association between activity and the number of P groups is seen during this reaction (Figure 16). The acidity of materials was determined by acid-base titration and the conversion was found to be dependent on P concentration. The most potent catalyst for fructose dehydration was found to be P-HHT CNFs, which also had the most acid sites and the highest P content[121].

4.3 Fine Chemical Synthesis

Porous structure and chemical surface of carbon materials provide appropriate environment allowing a wide range of relevant chemical transformations to take place. Several attempts have been reported on the use of nanocarbons in catalytic processes for the synthesis of fine chemicals including hydrogenation, condensation and various oxidation reactions[126].

A nanodiamond-based metal-free catalyst has been used for the first time for preparing N-rich heterocyclic compounds, particularly 1,3-triazoles, from benzonitriles under solvent-free conditions. The conventional acid-catalyzed route of this reaction, however, results in the formation of 1,2,4,5-tetrazines as a major product that has a different biological potential and ability for generating a new class of energetic compounds. Although, the chances of the progress of the reaction by this route are less but cannot be negated. The reaction with nanodiamonds (NDs) proceeds via hydrazine decomposition on ND surface leading to the formation of active N-centred radicals. These active N-centred radicals play a crucial role in activating the benzonitrile ring. The release of ammonia from hydrazine generates a reactive intermediate, imidogene (NH**), which triggers this reaction. The same reaction was also carried out with different aliphatic and aromatic nitriles (Benzonitriles, Pyridine-3-carbonitrile and 2-Furonitrile) as a substrate for their conversion into 3,5-disubstituted-4-amino-1,2,4-triazoles by utilizing ND as catalyst (Figure 17). It was observed that triazoles were obtained as a major product in all three substrates. Also, in the case of pyridine-3-carbonitrile, triazole was the only product with no other side products being formed. The exclusive yield of triazole product allows the application of this reaction on other molecules and opens the doors to industrial and synthetic applications[127].

A sulfonated carbon-based catalyst comprising amorphous carbon and nano graphite hybrids was prepared from the leaves of *Pinus roxburghii.* This catalyst was used for preparing N-substituted pyrrole derivatives via a C-N coupling reaction by two different pathways (Figure 18). Firstly, the reaction between benzoin, 2,4-dicarbonyl compounds and ammonium acetate was carried out for synthesizing tetrasubstituted pyrrole ring in the presence of a catalyst as a result, a series of N-substituted pyrrole derivatives were prepared. Secondly, the C-N coupling of primary amines with 2,5-dicarbonyl compounds was catalyzed by a carbon catalyst and another series of N-substituted pyrrole derivatives were prepared. The reaction appears to progress by the involvement of acidic sites present on the catalyst surface, which helped in the activation of carbonyl moiety. It was observed that a five-membered pyrrole nucleus is formed in excellent yields[128].

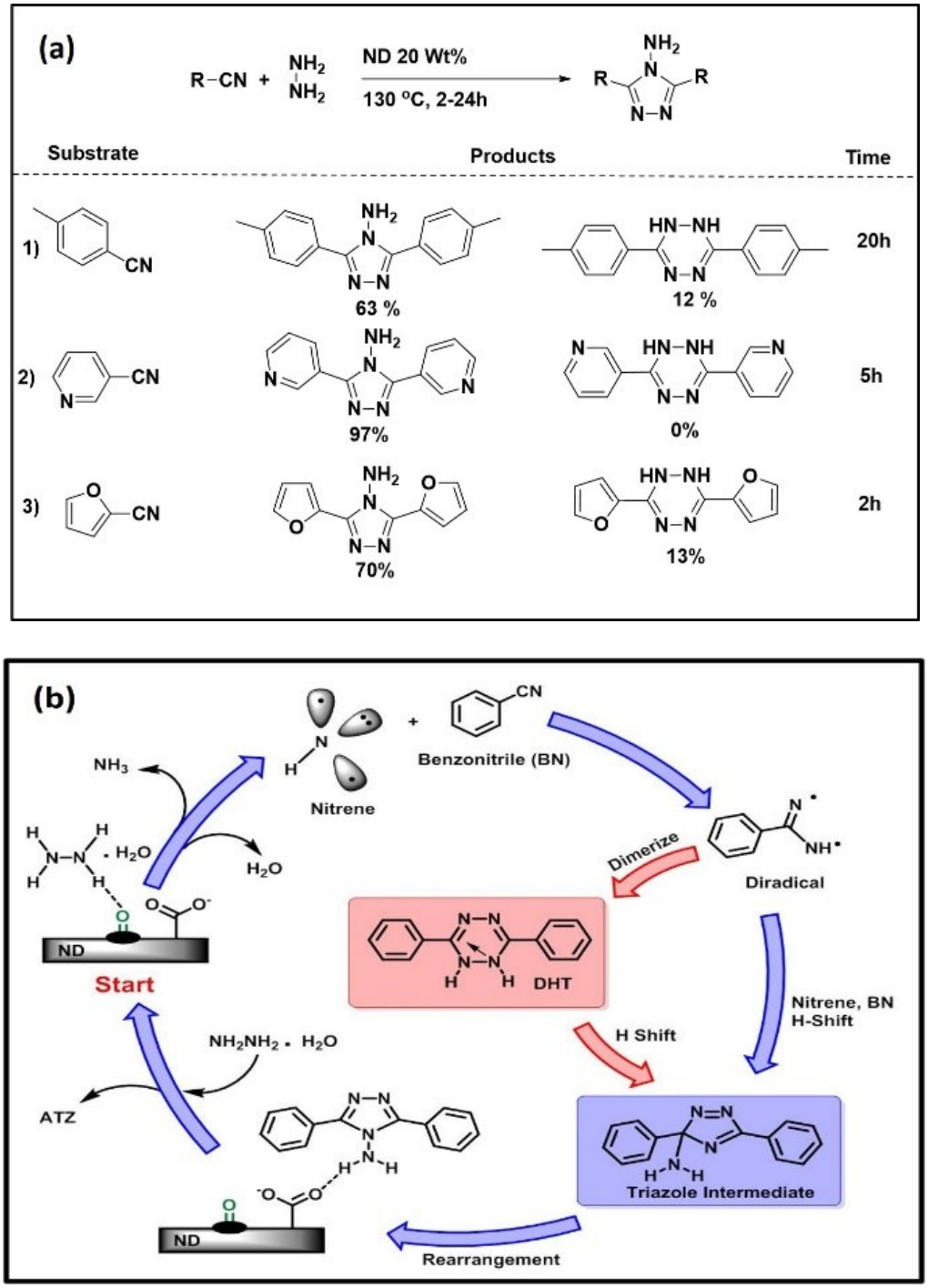

Figure 17. (a) Nanodiamond catalysed synthesis of triazoles **(b)** Mechanism involved in the reaction. Reprinted with permission from ref[127]. Copyright 2018 Elsevier Ltd. All rights reserved.

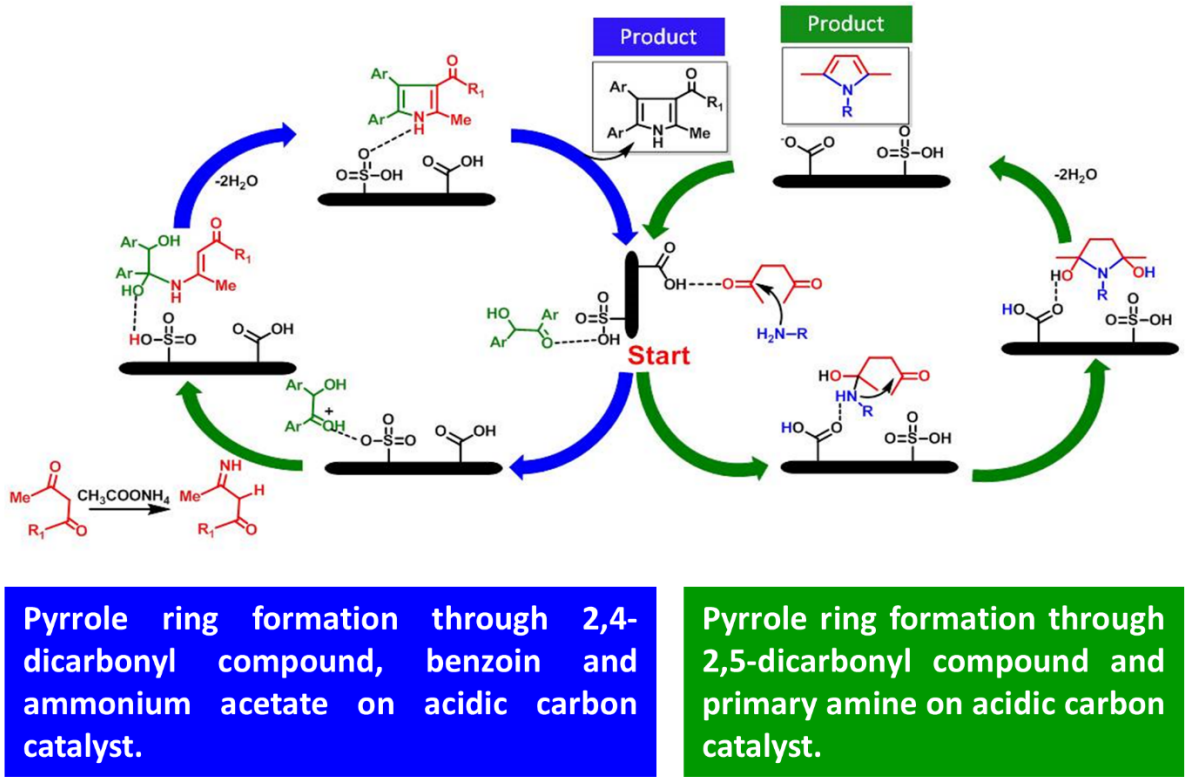

Figure 18. Probable mechanism for C-N coupling reaction. Reprinted with permission from ref[128]. Copyright 2017 Iranian Journal of Catalysis Ltd. All rights reserved.

A novel carbon-based catalyst (SO_3H-NSG)[129] implanted with sulfonic acid was designed by an ionic liquid-assisted doping technique and utilized for the synthesis of less toxic anticancer compounds. The introduction of sulphonic sites (SO_3H) on the catalyst surface starts the catalytic cycle where the carbonyl oxygen gets protonated. The reaction was carried out via 1,2 Michael addition with the kinetic product (1,2 addition products) being the major product (Scheme 4). The dominance of the 1,2-addition product confirms the regio-selectivity of the reaction with 1,2-product formation in large amounts than 1,4-addition products. Four different derivatives of coumarin-substituted bis(indolyl)methane were prepared and analyzed through FTIR and XPS techniques. Out of these, two novel N-protected derivatives were obtained. Hence, the toxicity/anti-cancer activities of these derivatives were tested with the help of computational and cytotoxicity studies. The developed synthetic protocol also benefited from low toxicity due to the use of a metal-free catalyst because there were no metal ions present in the process.

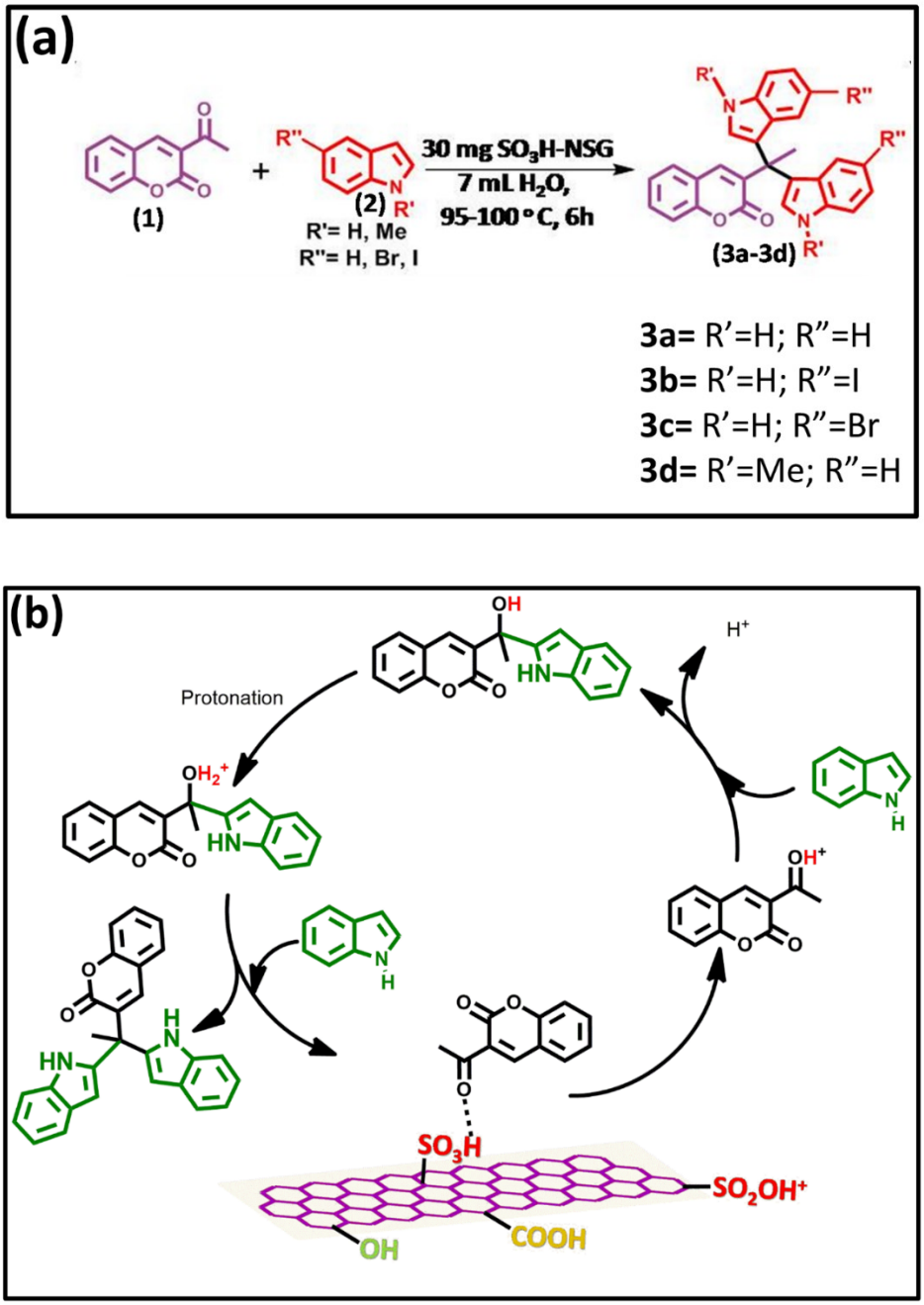

Scheme 4. (a) Synthetic scheme of coumarin substituted bis(indolyl)methanes catalysed by SO_3H-NSG. (b) Proposed mechanism for SO_3H-NSG catalysed synthesis of 3-(1,1-bis(3a,7a-dihydro-1H-indol-3-yl) ethyl)–2H-chromen-2-one. Reprinted with permission from ref[129]. Copyright 2021 Elsevier Ltd. All rights reserved.

The metal-free carbon-based catalysts have been widely used for the synthesis of N-rich heterocycles through either C-N or N-N coupling. These catalysts utilize the acidic active moieties present in their structure for various chemical conversions. The adjustable configuration, topological or structural defects and tuneable surface features of carbon

catalysts play a crucial role in catalyzing above reactions[130]. The scope of these carbon catalysts is not just limited to the synthesis of N-rich heterocycles. The introduction of nitrogen functionalities on carbon surface might enhance its catalytic performance[131]. Till now, there are wide varieties of nitrogen-functionalized carbon materials that have been used as metal-free catalysts in various reactions including C-H activation[132], electrocatalytic reduction of CO_2[133], oxygen reduction reactions (ORR)[134] and various oxidation reactions which include oxidation of alcohols[135], hydrogenation of nitroarenes[136] along with dehydrogenation of ethylbenzene[137]. In this continuation, efficient N rich carbon-based materials were prepared for different oxidation reactions.

A g-C_3N_4/graphite composite carbon material (g-C_3N_4@G) has been prepared by utilizing commercial graphite and urea as a source of nitrogen via wet impregnation method. Eventually, the prepared carbon material was used for the epoxidation of styrene as a metal-free catalyst (Figure 19a). The experimental results unquestionably support the solid catalyst's (g-C_3N_4@G) ability to promote styrene epoxidation to produce styrene oxide (uncatalyzed styrene oxidation produced only benzaldehyde). The peroxy radicals (*OOH) are probably stabilised by the carbon next to the sp^2 hybridised N, which is anticipated to be the reaction's key site. These radicals participate in the epoxidation of styrene to form styrene oxide[138]. GC-MS analysis was used to identify various side products in order to investigate the plausible reaction mechanism (Figure 19b). Aside from the main oxidation products (benzaldehyde and styrene oxide), the other products were diphenylethanedione, 1-phenyl, benzoic acid and 1,2-ethanediol. Side products are unavoidable because of alternate reaction pathways provided by the C=C reactive sites[139]. Further evidence for the g-C_3N_4 sheets' active role in styrene epoxidation came from a linear relationship between catalytic performance and the number of sp^2 hybridised N-sites in the sheets. [140].

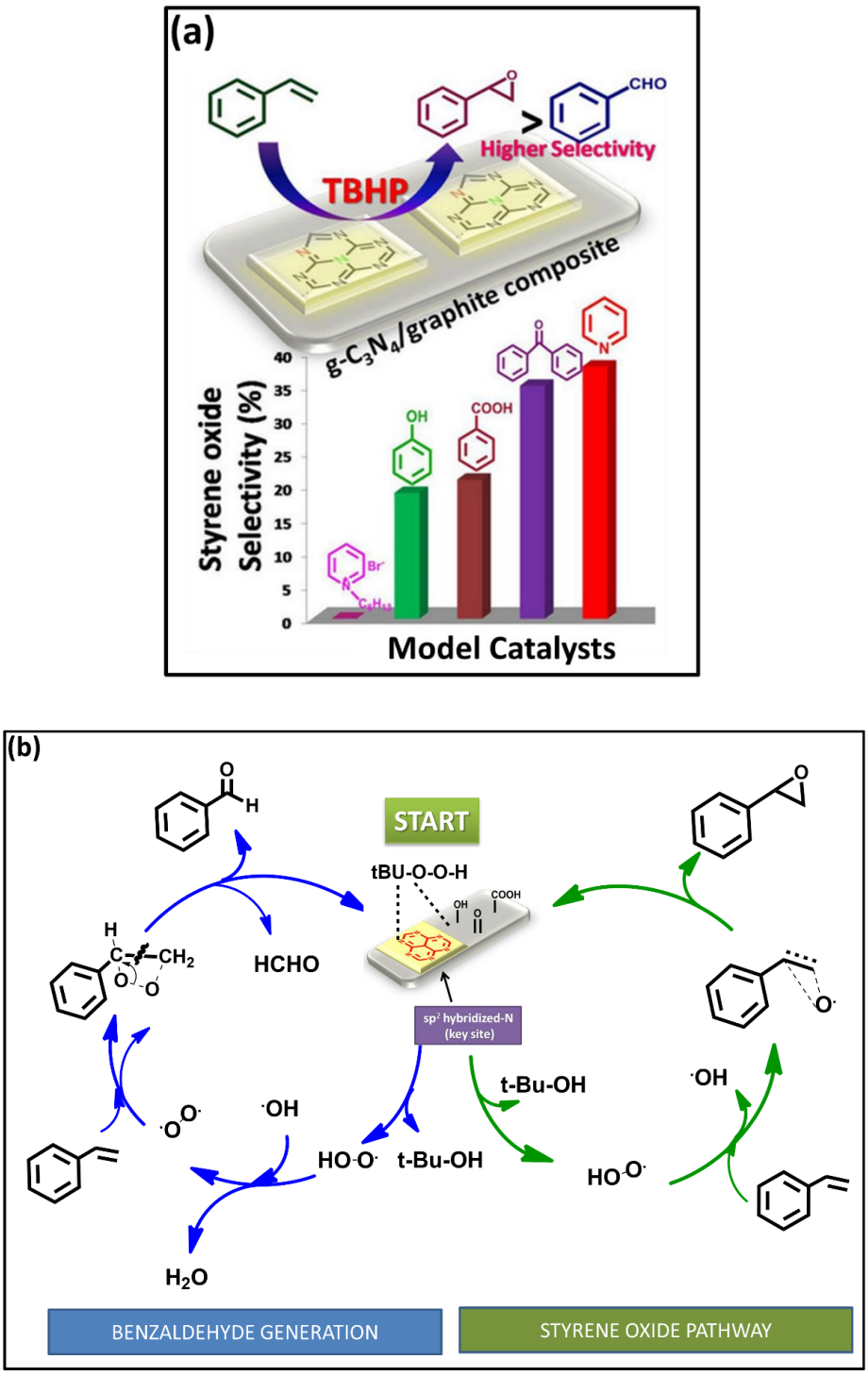

Figure 19. (a) Synthetic pathway of g-C3N4 modified graphite for selective styrene-to-styrene oxide oxidation (b) Proposed catalytic pathways for styrene oxidation to styrene oxide and benzaldehyde using g-C_3N_4@G as a catalyst**.** Reprinted with permission from ref[140]. Copyright 2021 Wiley Ltd. All rights reserved.

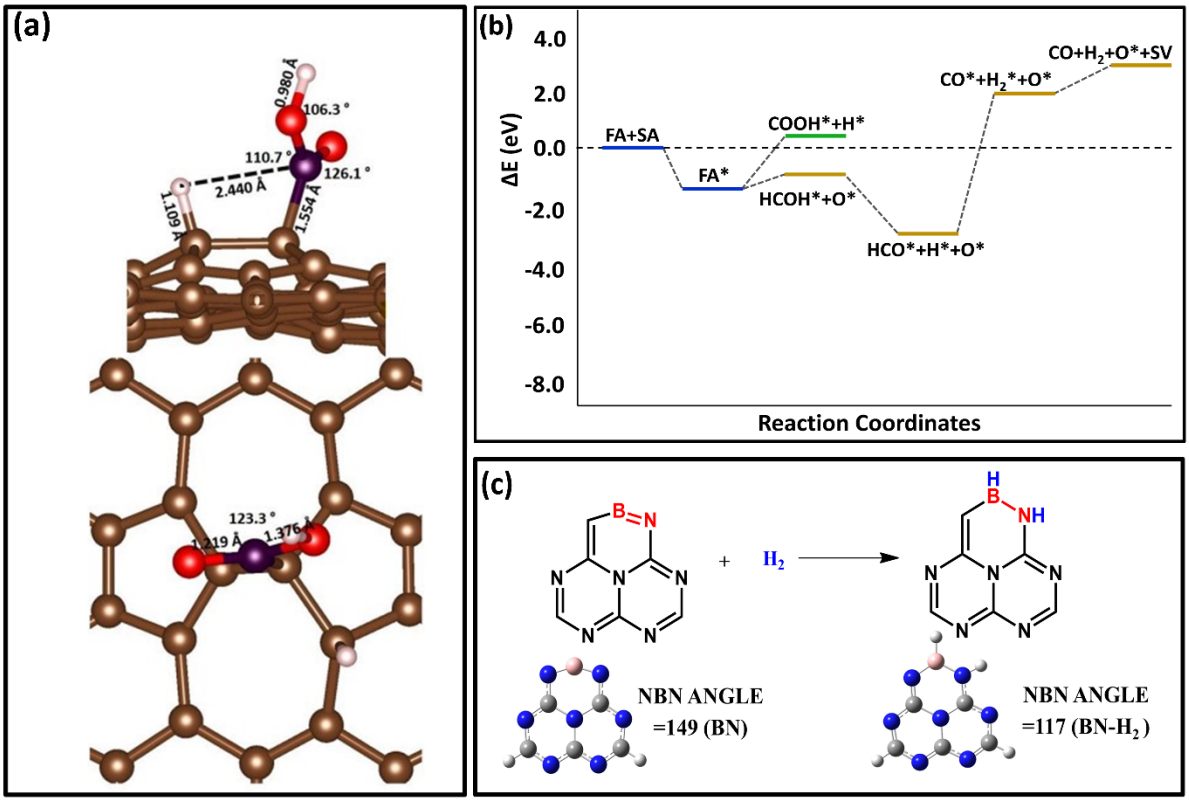

Figure 20. (a) Dissociative adsorption of formic acid on Stone-Wales defect (SW1) (b) Energy profile demonstrating various pathways for the decomposition of Formic Acid on single-vacancy (SV) structure (c) The reaction of boron nitride with hydrogen gas. Angle strains are depicted in three dimensional figures before and after the reaction. Reprinted with permission from ref7,142. Copyright 2020 Royal Society of Chemistry. All rights reserved.

For the liquid phase dehydrogenation of formic acid (FA) into CO and H_2, graphite oxide (GO), commercial graphite (GP) along with carbon nanofibers (CNF-PR24-PS and CNF-PR24-LHT) were utilized as metal-free carbon catalysts. The results of XPS and Raman analysis revealed that the activity of prepared catalyst is directly related to the defects of carbon material. Particularly, FA decomposition increases with an increase in defects of the material in the order GO > CNF-PR24-PS > CNF-PR24-LHT > GP. A linear correlation between defects and FA conversion (R^2=0.99) was found but no such direct correlation was observed for oxygen functionalities. To better understand the role of the various types of defects, the decomposition of formic acid was studied employing DFT models of pristine graphene along with various defective graphene surfaces such as single or double vacancies and various Stone-Wales defects (Figure 20 a). It was demonstrated that not all defects act as active sites for formic acid adsorption and decomposition. The activity is primarily due to the single

vacancy defect since because of its capability of decomposing formic acid into gaseous molecules and recycling the active site. Two distinct pathways were discovered, one through carboxyl species and the other via a hydroxy methylene intermediate (Figure 20 b). In both mechanisms, an intermediate species like CO or atomic hydrogen poisoned the active sites, which accounts for the catalyst deactivation seen in the experimental results[141].

Besides oxidation reactions, these metal-free carbon catalysts can also be used in various reduction reactions leading to fine chemical synthesis. In both academia and industry, catalytic hydrogenation of unsaturated compounds with molecular hydrogen has a wide range of applications. Metal-free carbon materials acting as heterogeneous catalysts for hydrogenation of carbon dioxide[143] and nitroarenes[144] have recently been reported. Despite research in the field of metal-free free heterogeneous catalysis for hydrogenation reactions[145], it is still necessary to develop sustainable catalysts in order to keep chemical processes sustainable.

A Lewis base, carbon nitride has been widely utilized in a large number of chemical transformations as a heterogeneous and sustainable metal-free catalyst because of its relatively affordable cost, desired chemical stability and recyclability[146–148]. Two metal-free heterogeneous catalysts containing B-doped graphitic carbon nitride having both Lewis acidic (B) and Lewis basic (N) sites were synthesized for the liquid phase styrene hydrogenation under mild conditions. The results show that incorporating B into the g-C_3N_4 matrix increases activity significantly. According to DFT calculations, when a B atom enters the matrix as a pi-bonded component, the ring strain in the molecule causes the hydrogen molecule to cleave, which causes hydrogenation (Figure 20 c). Furthermore, incorporating a B-atom with a F-atom (highly electronegativity) may not improve the behavior of active sites toward H_2 cleavage. The developed method offers softer operational conditions than previously reported methods[142].

5. Future Perspectives

There are still many obstacles to overcome before carbon-based catalysts may fully replace metal-based counterparts. The use of these carbo-catalysts in industrial applications including energy storage, sensing and fine chemical synthesis need to be emphasized. Key reactions and materials need to be identified. With the help of industries, key active sites

need to be designed and controlled for specific applications. Also, the incorporation of heteroatoms in carbon materials has to be done in such a manner that does not alter the material surface properties. Although long-term durability, particularly in practical devices, has not been confirmed using standard assessment techniques, the position of heteroatoms in carbon-based catalysts and their actual catalytic role are still unknown. The inability to accurately control active sites and difficulties in defining active-site structures can lead to the poor performance of the designed catalysts. To precisely regulate the position, concentration and distribution of active sites in carbon catalysts, novel synthetic and/or doping techniques must be devised. However, these inventive approaches and progress highlighted in this account is an important step in sensor development leading towards efficient and effective POC devices to provide cheap and affordable healthcare facilities to the user end. Recent developments, emerging challenges, and some insights on the fabrication of heteroatom-doped carbon materials as metal-free catalysts have given them great promise. These materials in particular hold great promise for a variety of application, including sensing, energy storage and fine chemical synthesis in the near future.

6. Conclusion

Recent research trends have advanced the subtle implementation of materials designing and surface science fundamentals to achieve highly efficient metal-free carbon-based catalytic systems with enticing synergistic effects. Different techniques such as electrospinning, thermal annealing, covalent tagging and heteroatom doping have been used for incorporating various key active sites in the metal-free carbon materials. These methodologies have been used for the synthesis of metal-free carbo-catalysts with novel physicochemical properties demonstrating efficient catalytic activities toward electrochemical sensing, biomass valorization and fine chemical synthesis. A combination of experimental and theoretical studies has also been used to direct the fabrication of highly active carbo-catalysts and reveal reaction pathways. The ultimate goal is to create low-cost, high-performance carbo-catalysts for sensing of body fluids along with conversion of waste biomass into valuable products and fine chemicals. We have discussed in this account in detail the latest developments in fabrication of metal-free carbon-based catalysts, primarily on the basis of our efforts in the past 7 years. Significant progress in improving catalyst

activity/stability and promising performance has been made, bringing metal-free carbo-catalyst technology closer to potentially viable applications in the near future.

Author Contribution

The research work of NG and AV was compiled by VBJ. The idea was collectively finalised by NG and AV. NG was involved in all stages of work starting from planning to writing of this manuscript. VBJ wrote the manuscript in close association with NG and AV has revised it. VBJ has drawn the figures including graphical abstract (besides the figures for which copyright permissions were sought).

Conflicts of Interest

There are no conflicts to declare.

References

1 R. Patnaik, in *IOP Conference Series: Earth and Environmental Science*, Institute of Physics Publishing, 2018, vol. 120.

2 A. Dogra and N. Gupta, *ChemistrySelect*, 2019, 4, 10452–10465.

3 X. K. Kong, C. le Chen and Q. W. Chen, *Chem Soc Rev*, 2014, 43, 2841–2857.

4 D. S. Su, J. Zhang, B. Frank, A. Thomas, X. Wang, J. Paraknowitsch and R. Schlögl, *ChemSusChem*, 2010, 3, 169–180.

5 A. Primo, V. Parvulescu and H. Garcia, *Journal of Physical Chemistry Letters*, 2017, 8, 264–278.

6 X. Liu and L. Dai, *Nat Rev Mater*, 2016, 1.

7 I. Barlocco, S. Capelli, X. Lu, S. Tumiati, N. Dimitratos, A. Roldan and A. Villa, *Nanoscale*, 2020, **12**, 22768–22777.

8 M. M. Titirici and M. Antonietti, *Chem Soc Rev*, 2010, **39**, 103–116.

9 B. Yin, E. Zhao, X. Hua, K. Wang, W. Wang, G. Li and T. Liu, *New Journal of Chemistry*, 2020, **44**, 2011–2015.

10 X. F. Yang, A. Wang, B. Qiao, J. Li, J. Liu and T. Zhang, *Acc Chem Res*, 2013, **46**, 1740–1748.

11 Biochemische Zeitschrift in Search Works catalog, https://searchworks.stanford.edu/view/353734, (accessed 12 February 2023).

12 M. Monai, M. Melchionna and P. Fornasiero, in *Advances in Catalysis*, Academic Press Inc., 2018, vol. 63, pp. 1–73.

13 J. Zhang, D. Su, A. Zhang, D. Wang, R. Schlögl and C. Hébert, *Angewandte Chemie - International Edition*, 2007, **46**, 7319–7323.

14 C. Su, M. Acik, K. Takai, J. Lu, S. J. Hao, Y. Zheng, P. Wu, Q. Bao, T. Enoki, Y. J. Chabal and K. P. Loh, *Nat Commun*, , DOI:10.1038/ncomms2315.

15 D. S. Su, J. Zhang, B. Frank, A. Thomas, X. Wang, J. Paraknowitsch and R. Schlögl, *ChemSusChem*, 2010, 3, 169–180.

16 B. F. MacHado and P. Serp, *Catal Sci Technol*, 2012, 2, 54–75.

17 B. Li and Z. Xu, *J Am Chem Soc*, 2009, **131**, 16380–16382.

18 D. R. Dreyer, H.-P. Jia and C. W. Bielawski, *Angewandte Chemie*, 2010, **122**, 6965–6968.

19 S. Navalon, A. Dhakshinamoorthy, M. Alvaro and H. Garcia, *Coord Chem Rev*, 2016, 312, 99–148.

20 S. Navalon, A. Dhakshinamoorthy, M. Alvaro, M. Antonietti and H. García, *Chem. Soc. Rev.*, 2017, **46**, 4501–4529.

21 O. Vaughan, *Nature Nanotechnology 2016*, 2016, 1–1.

22 J. Xu, Y. Zhao, C. Shen and L. Guan, *ACS Appl Mater Interfaces*, 2013, **5**, 12594–12601.

23 Z. M. Huang, Y. Z. Zhang, M. Kotaki and S. Ramakrishna, *Compos Sci Technol*, 2003, **63**, 2223–2253.

24 A. Greiner and J. H. Wendorff, *Angewandte Chemie - International Edition*, 2007, 46, 5670–5703.

25 E. A. M. Hassan, T. H. H. Elagib, H. Memon, M. Yu and S. Zhu, *Materials (Basel)*, , DOI:10.3390/MA12050778.

26 Y. Ding, B. Zhang, N. Gupta and D. S. Su, *Green Chemistry*, 2015, **17**, 1107–1112.

27 K. R. D. Kasibhatta, I. Madakannu and I. Prasanthi, *J Inorg Organomet Polym Mater*, 2021, **31**, 1859–1876.

28 A. Ojha, D. Tiwary, R. Oraon and P. Singh, *Environmental Science and Pollution Research*, 2021, **28**, 30573–30594.

29 A. Villa, J. P. Tessonnier, O. Majoulet, D. S. Su and R. Schlögl, *ChemSusChem*, 2010, **3**, 241–245.

30 A. Dogra, V. Sharma, I. Barlocco, A. Villa and N. Gupta, *New Journal of Chemistry*, 2021, **45**, 19651–19654.

31 J. J. Feng, *Physics of Fluids*, 2002, **14**, 3912–3926.

32 B. Barua and M. C. Saha, *Polym Eng Sci*, 2018, **58**, 998–1009.

33 D. H. Reneker and I. Chun, *Nanometre diameter fibres of polymer, produced by electrospinning*, 1996, vol. 7.

34 D. Li, A. Babel, S. A. Jenekhe and Y. Xia, *Advanced Materials*, 2004, **16**, 2062–2066.

35 K. Acatay, E. Simsek, C. Ow-Yang and Y. Z. Menceloglu, *Angewandte Chemie*, 2004, **116**, 5322–5325.

36 Y. Z. Jin, Y. J. Kim, C. Gao, Y. Q. Zhu, A. Huczko, M. Endo and H. W. Kroto, *Carbon N Y*, 2006, **44**, 724–729.

37 Y. Z. Jin, Y. J. Kim, C. Gao, Y. Q. Zhu, A. Huczko, M. Endo and H. W. Kroto, *Carbon N Y*, 2006, **44**, 724–729.

38 F. von Sturm, *Advanced Materials*, 1989, **1**, 130–131.

39 Y. A. Kim, T. Hayashi, K. Osawa, M. S. Dresselhaus and M. Endo, *Chem Phys Lett*, 2003, **380**, 319–324.

40 C. C. Han, J. T. Lee and H. Chang, *Chemistry of Materials*, 2001, **13**, 4180–4186.

41 V. Bharati Jaryal, D. Singh and N. Gupta, *New Journal of Chemistry*, 2022, **46**, 5712–5718.

42 C. Liang, Z. Li and S. Dai, *Angewandte Chemie - International Edition*, 2008, 47, 3696–3717.

43 D. Tasis, N. Tagmatarchis, V. Georgakilas and M. Prato, *Chemistry – A European Journal*, 2003, **9**, 4000–4008.

44 A. Hirsch, *Angew. Chem. Int. Ed*, DOI:10.1002/1521-3773.

45 N. I. Kovtyukhova, T. E. Mallouk, L. Pan and E. C. Dickey, *J Am Chem Soc*, 2003, **125**, 9761–9769.

46 W. Zhao, C. Song and P. E. Pehrsson, *J Am Chem Soc*, 2002, **124**, 12418–12419.

47 K. Yang and B. Xing, *Chem Rev*, 2010, **110**, 5989–6008.

48 C. A. Dyke and J. M. Tour, *Journal of Physical Chemistry A*, 2004, **108**, 11151–11159.

49 J. E. Fischer, *Acc Chem Res*, 2002, **35**, 1079–1086.

50 Z. M. Dang, L. Wang and L. P. Zhang, *J Nanomater*, 2006, **2006**, 1–5.

51 J. P. Paraknowitsch and A. Thomas, *Energy Environ Sci*, 2013, **6**, 2839–2855.

52 L. Dai, Y. Xue, L. Qu, H. J. Choi and J. B. Baek, *Chem Rev*, 2015, **115**, 4823–4892.

53 C. Hu and L. Dai, *Advanced Materials*, 2019, **31**, 1804672.

54 K. das Sen and C. K. Jørgensen, Eds., , DOI:10.1007/BFB0029833.

55 J. Zhang and L. Dai, *ACS Catal*, 2015, **5**, 7244–7253.

56 L. Dai, *Acc Chem Res*, 2013, **46**, 31–42.

57 H. Wang, Y. Shao, S. Mei, Y. Lu, M. Zhang, J. K. Sun, K. Matyjaszewski, M. Antonietti and J. Yuan, *Chem Rev*, 2020, **120**, 9363–9419.

58 H. Wang, Y. Shao, S. Mei, Y. Lu, M. Zhang, J. K. Sun, K. Matyjaszewski, M. Antonietti and J. Yuan, *Chem Rev*, 2020, **120**, 9363–9419.

59 A. E. C. Collis and I. T. Horváth, *Catal Sci Technol*, 2011, **1**, 912–919.

60 J. H. Kim, J. W. Kim, M. Shokouhimehr and Y. S. Lee, *Journal of Organic Chemistry*, 2005, **70**, 6714–6720.

61 G. Panomsuwan, N. Saito and T. Ishizaki, *ACS Appl Mater Interfaces*, 2016, **8**, 6962–6971.

62 S. Ratso, I. Kruusenberg, M. Vikkisk, U. Joost, E. Shulga, I. Kink, T. Kallio and K. Tammeveski, *Carbon N Y*, 2014, **73**, 361–370.

63 P. Chen, T. Y. Xiao, Y. H. Qian, S. S. Li and S. H. Yu, *Advanced Materials*, 2013, **25**, 3192–3196.

64 Y. Zhang, W. J. Jiang, X. Zhang, L. Guo, J. S. Hu, Z. Wei and L. J. Wan, *Physical Chemistry Chemical Physics*, 2014, **16**, 13605–13609.

65 H. T. Chung, J. H. Won and P. Zelenay, *Nature Communications 2013 4:1*, 2013, **4**, 1–5.

66 J. Qian, F. Wu, Y. Ye, M. Zhang, Y. Huang, Y. Xing, W. Qu, L. Li and R. Chen, *Adv Energy Mater*, 2018, **8**, 1703159.

67 Z. Wang, W. Xu, X. Chen, Y. Peng, Y. Song, C. Lv, H. Liu, J. Sun, D. Yuan, X. Li, X. Guo, D. Yang and L. Zhang, *Adv Funct Mater*, 2019, **29**, 1902875.

68 R. Guo, C. Lv, W. Xu, J. Sun, Y. Zhu, X. Yang, J. Li, J. Sun, L. Zhang and D. Yang, *Adv Energy Mater*, 2020, **10**, 1903652.

69 K. Bala, D. Sharma and N. Gupta, *ChemElectroChem*, 2019, **6**, 274–288.

70 D. M. Fouad and W. A. El-Said, *J Nanomater*, , DOI:10.1155/2016/6194230.

71 L. I. N. Tomé and C. M. A. Brett, *Electroanalysis*, 2019, **31**, 704–710.

72 J. Tashkhourian, S. F. Nami-Ana and M. Shamsipur, *J Mol Liq*, 2018, **266**, 548–556.

73 X. Liu, L. Luo, Y. Ding, Q. Wu, Y. Wei and D. Ye, *Journal of Electroanalytical Chemistry*, 2012, **675**, 47–53.

74 W. Ren, H. Q. Luo and N. B. Li, *Sensors 2006, Vol. 6, Pages 80-89*, 2006, **6**, 80–89.

75 K. Bala, J. Suriyaprakash, P. Singh, K. Chauhan, A. Villa and N. Gupta, *New Journal of Chemistry*, 2018, **42**, 6604–6608.

76 N. G. Mphuthi, A. S. Adekunle and E. E. Ebenso, *Scientific Reports 2016 6:1*, 2016, **6**, 1–20.

77 M. Mazloum-Ardakani, F. Farbod and L. Hosseinzadeh, *Journal of Nanostructures*, 2016, **6**, 293–300.

78 M. E. Ghica and C. M. A. Brett, *https://doi.org/10.1080/00032719.2012.762584*, 2013, **46**, 1379–1393.

79 K. Koteshwara Reddy, M. Satyanarayana, K. Yugender Goud, K. Vengatajalabathy Gobi and H. Kim, *Materials Science and Engineering: C*, 2017, **79**, 93–99.

80 H. MahmoudiMoghaddam, H. Beitollahi, S. Tajik and H. Soltani, *Electroanalysis*, 2015, **27**, 2620–2628.

81 H. Kang, Y. Jin and Q. Han, *http://dx.doi.org/10.1080/00032719.2013.876541*, 2014, **47**, 1552–1563.

82 X. Li, M. Chen and X. Ma, *Analytical Sciences*, 2012, **28**, 147–147.

83 X. Ma, M. Chao and Z. Wang, *Analytical Methods*, 2012, **4**, 1687–1692.

84 S. Sun, X. Gou, S. Tao, J. Cui, J. Li, Q. Yang, S. Liang and Z. Yang, *Mater Chem Front*, 2019, **3**, 597–605.

85 S. Jawaid, F. N. Talpur, H. I. Afridi, S. M. Nizamani, A. A. Khaskheli and S. Naz, *Analytical Methods*, 2014, **6**, 5269–5273.

86 K. Sen, S. Ali, D. Singh, K. Singh and N. Gupta, *FlatChem*, 2021, **30**, 100288.

87 J. Suriyaprakash, L. Shan, N. Gupta, H. Wang and L. Wu, *Compos B Eng*, 2022, **245**, 110233.

88 J. Suriyaprakash, N. Gupta, L. Wu and L. Shan, *Chemical Engineering Journal*, 2022, **436**, 135254.

89 Y. Lei, D. Butler, M. C. Lucking, F. Zhang, T. Xia, K. Fujisawa, T. Granzier-Nakajima, R. Cruz-Silva, M. Endo, H. Terrones, M. Terrones and A. Ebrahimi, *Sci Adv*, 2020, **6**, 4250–4257.

90 N. Gupta, G. A. Kaur, V. Sharma, R. Nagraik and M. Shandilya, *Journal of Electroanalytical Chemistry*, 2022, **904**, 115904.

91 J. Suriyaprakash, K. Bala, L. Shan, L. Wu and N. Gupta, *ACS Appl Mater Interfaces*, 2021, **13**, 60878–60893.

92 P. Puthongkham and B. J. Venton, *ACS Sens*, 2019, **4**, 2403–2411.

93 J. Suriyaprakash, K. Bala, L. Shan, L. Wu and N. Gupta, *ACS Appl Mater Interfaces*, 2021, **13**, 60878–60893.

94 M. L. Yola and N. Atar, *Compos B Eng*, 2019, **175**, 107113.

95 S. Fatma, B. B. Prasad, S. Jaiswal, R. Singh and K. Singh, *Biosens Bioelectron*, 2019, **135**, 36–44.

96 J. Suriyaprakash, N. Gupta, L. Shan and L. Wu, *Adv Mater Technol*, 2022, **7**, 2200099.

97 J. Suriyaprakash, N. Gupta, L. Shan and L. Wu, *Adv Mater Technol*, 2022, **7**, 2200099.

98 L. Appels and R. Dewil, *Resour Conserv Recycl*, 2012, **59**, 1–3.

99 S. I. Martínez-Guido, I. M. Ríos-Badrán, C. Gutiérrez-Antonio and J. M. Ponce-Ortega, *Renew Energy*, 2019, **130**, 622–632.

100 Y. Gao, X. Gao and X. Zhang, *Engineering*, 2017, **3**, 272–278.

101 V. V. Kumar, A. Hoadley and Y. Shastri, *Sustain Prod Consum*, 2019, **18**, 165–178.

102 E. Pfab, L. Filiciotto and R. Luque, *J Chem Educ*, 2019, **96**, 3030–3037.

103 E. Cséfalvay and I. T. Horváth, *ACS Sustain Chem Eng*, 2018, **6**, 8868–8874.

104 L. Filiciotto and R. Luque, *Current Green Chemistry*, 2018, **5**, 47–59.

105 L. Wu, T. Moteki, A. A. Gokhale, D. W. Flaherty and F. D. Toste, *Chem*, 2016, **1**, 32–58.

106 World population projected to reach 9.8 billion in 2050, and 11.2 billion in 2100 | UN DESA | United Nations Department of Economic and Social Affairs, https://www.un.org/development/desa/en/news/population/world-population-prospects-2017.html, (accessed 15 January 2023).

107 F. D. Pileidis and M. M. Titirici, *ChemSusChem*, 2016, **9**, 562–582.

108 Z. Sun, B. Fridrich, A. de Santi, S. Elangovan and K. Barta, *Chem Rev*, 2018, **118**, 614–678.

109 J. J. Bozell and G. R. Petersen, *Green Chemistry*, 2010, **12**, 539–554.

110 N. Gupta, O. Khavryuchenko, A. Villa and D. Su, *ChemSusChem*, 2017, **10**, 3030–3034.

111 Y. Gao, G. Hu, J. Zhong, Z. Shi, Y. Zhu, D. S. Su, J. Wang, X. Bao and D. Ma, *Angewandte Chemie International Edition*, 2013, **52**, 2109–2113.

112 Y. Lin and D. Su, *ACS Nano*, 2014, **8**, 7823–7833.

113 P. Mäki-Arvela, B. Holmbom, T. Salmi and D. Y. Murzin, *Catalysis Reviews*, 2007, **49**, 197–340.

114 G. W. Huber, S. Iborra and A. Corma, *Chem Rev*, 2006, **106**, 4044–4098.

115 A. Corma Canos, S. Iborra and A. Velty, *Chem Rev*, 2007, **107**, 2411–2502.

116 A. M. Ruppert, J. D. Meeldijk, B. W. M. Kuipers, B. H. Erné and B. M. Weckhuysen, *Chemistry – A European Journal*, 2008, **14**, 2016–2024.

117 Y. Liu, E. Lotero, J. G. Goodwin and C. Lu, *J Catal*, 2007, **246**, 428–433.

118 J. P. Tessonnier, A. Villa, O. Majoulet, D. S. Su and R. Schlögl, *Angewandte Chemie International Edition*, 2009, **48**, 6543–6546.

119 D. G. Cantrell, L. J. Gillie, A. F. Lee and K. Wilson, *Appl Catal A Gen*, 2005, **287**, 183–190.

120 A. Villa, J. P. Tessonnier, O. Majoulet, D. S. Su and R. Schlögl, *Chemical Communications*, 2009, 4405–4407.

121 S. Campisi, F. J. S. Trujillo, D. Motta, T. E. Davies, N. Dimitratos and A. Villa, *C 2018, Vol. 4, Page 9*, 2018, **4**, 9.

122 A. Villa, M. Schiavoni, P. F. Fulvio, S. M. Mahurin, S. Dai, R. T. Mayes, G. M. Veith and L. Prati, *Journal of Energy Chemistry*, 2013, **22**, 305–311.

123 C. Carlini, P. Patrono, A. M. R. Galletti and G. Sbrana Glauco, *Appl Catal A Gen*, 2004, **275**, 111–118.

124 Y. Zhang, J. Wang, J. Ren, X. Liu, X. Li, Y. Xia, G. Lu and Y. Wang, *Catal Sci Technol*, 2012, **2**, 2485–2491.

125 P. Carniti, A. Gervasini, S. Biella and A. Auroux, *Catal Today*, 2006, **118**, 373–378.

126 E. Pérez-Mayoral, I. Matos, M. Bernardo and I. M. Fonseca, *Catalysts 2019, Vol. 9, Page 133*, 2019, **9**, 133.

127 N. Gupta, O. Khavryuchenko, G. Wen, K. H. Wu and D. Su, *Carbon N Y*, 2018, **130**, 714–723.

128 N. Gupta, P. Bhardwaj and A. Kumar, *Iranian Journal of Catalysis*, 2017, **7**, 171–179.

129 V. Singh, A. Dogra, J. Das, P. Manna and N. Gupta, *FlatChem*, 2021, **29**, 100279.

130 D. S. Su, J. Zhang, B. Frank, A. Thomas, X. Wang, J. Paraknowitsch and R. Schlögl, *ChemSusChem*, 2010, **3**, 169–180.

131 R. Liu, D. Wu, X. Feng, K. Müllen, R. Liu, D. Wu, X. Feng and K. Müllen, *Angewandte Chemie*, 2010, **122**, 2619–2623.

132 Y. Lin, Z. Liu, L. Yu, G. R. Zhang, H. Tan, K. H. Wu, F. Song, A. K. Mechler, P. P. M. Schleker, Q. Lu, B. Zhang and S. Heumann, *Angewandte Chemie International Edition*, 2021, **60**, 3299–3306.

133 D. M. Fernandes, A. F. Peixoto and C. Freire, *Dalton Transactions*, 2019, **48**, 13508–13528.

134 H. Jiang, J. Gu, X. Zheng, M. Liu, X. Qiu, L. Wang, W. Li, Z. Chen, X. Ji and J. Li, *Energy Environ Sci*, 2019, **12**, 322–333.

135 Y. Cui, Y. H. Lee and J. W. Yang, *Scientific Reports 2017 7:1*, 2017, **7**, 1–9.

136 J. Shan, X. Sun, S. Zheng, T. Wang, X. Zhang and G. Li, *Carbon N Y*, 2019, **146**, 60–69.

137 Y. Liu, H. Ba, J. Luo, K. H. Wu, J. M. Nhut, D. S. Su and C. Pham-Huu, *Catal Today*, 2018, **301**, 38–47.

138 H. Fu, K. Huang, G. Yang, Y. Cao, H. Wang, F. Peng, Q. Wang and H. Yu, *ACS Catal*, 2020, **10**, 129–137.

139 A. Dhakshinamoorthy, A. Primo, P. Concepcion, M. Alvaro and H. Garcia, *Chemistry – A European Journal*, 2013, **19**, 7547–7554.

140 A. Dogra, A. Kumar, M. Kapoor and N. Gupta, *ChemistrySelect*, 2021, **6**, 7118–7122.

141 I. Barlocco, S. Capelli, X. Lu, S. Tumiati, N. Dimitratos, A. Roldan and A. Villa, *Nanoscale*, 2020, **12**, 22768–22777.

142 A. Dogra, I. Barlocco, A. Singh, F. Somodi, A. Villa and N. Gupta, *Catal Sci Technol*, 2020, **10**, 3024–3028.

143 J. Wu, C. Wen, X. Zou, J. Jimenez, J. Sun, Y. Xia, M. T. Fonseca Rodrigues, S. Vinod, J. Zhong, N. Chopra, I. N. Odeh, G. Ding, J. Lauterbach and P. M. Ajayan, *ACS Catal*, 2017, **7**, 4497–4503.

144 R. Gao, L. Pan, J. Lu, J. Xu, X. Zhang, L. Wang and J. J. Zou, *ChemCatChem*, 2017, **9**, 4287–4294.

145 Y. Ding, X. Huang, X. Yi, Y. Qiao, X. Sun, A. Zheng and D. S. Su, *Angewandte Chemie International Edition*, 2018, **57**, 13800–13804.

146 F. Goettmann, A. Fischer, M. Antonietti and A. Thomas, *Chemical Communications*, 2006, 4530–4532.

147 X. H. Li, X. Wang and M. Antonietti, *ACS Catal*, 2012, **2**, 2082–2086.

148 J. Zhu, Y. Wei, W. Chen, Z. Zhao and A. Thomas, *Chemical Communications*, 2010, **46**, 6965–6967.